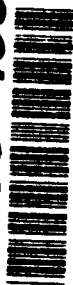# NAVAL POSTGRADUATE SCHOOL
Monterey, California

THESIS

SDTIC
ELECTE
AUG 19, 1994
B D

SHALLOW WATER
REVERBERATION
MEASUREMENT AND PREDICTION

by

Charles E. Muggleworth

June, 1994

Thesis Advisors: James H. Miller
                                    Ching-Sang Chiu

Approved for public release; distribution is unlimited.

94 8 18 160

DTIC QUALITY INSPECTED 1

REPORT DOCUMENTATION PAGE

Form Approved OMB No. 0704-0188

1. AGENCY USE ONLY *(Leave blank)*	2. REPORT DATE June 1994	3. REPORT TYPE AND DATES COVERED Master's Thesis

4. TITLE AND SUBTITLE
SHALLOW WATER REVERBERATION MEASUREMENT AND PREDICTION

5. FUNDING NUMBERS

6. AUTHOR(S)
Charles E. Muggleworth

7. PERFORMING ORGANIZATION NAME(S) AND ADDRESS(ES)
Naval Postgraduate School
Monterey CA 93943-5000

8. PERFORMING ORGANIZATION REPORT NUMBER

9. SPONSORING/MONITORING AGENCY NAME(S) AND ADDRESS(ES)

10. SPONSORING/MONITORING AGENCY REPORT NUMBER

11. SUPPLEMENTARY NOTES The views expressed in this thesis are those of the author and do not reflect the official policy or position of the Department of Defense or the U.S. Government.

12a. DISTRIBUTION/AVAILABILITY STATEMENT Approved for public release; distribution is unlimited.	12b. DISTRIBUTION CODE A

13. ABSTRACT *(maximum 200 words)*
Low frequency active sonar performance in shallow water is often limited by reverberation. Reverberation modeling in shallow water has been difficult due to the complexity of the multipath acoustic propagation problem inherent in shallow environments. In August 1992, a shallow water, low-frequency reverberation measurement was made in the Barents Sea utilizing explosive "signal, underwater sound" (SUS) charges as sound sources and a 16-element vertical hydrophone array as the receiver. The objectives of this thesis were to analyze the reverberation data from this experiment, compare several theories which have been proposed to model reverberation, and determine the reverberant characteristics of the region. The three-dimensional Hamiltonian Acoustic Ray-tracing Program for the Ocean (HARPO) was used as the primary propagation modeling tool. The temporal signal processing consisted of a short-time Fourier transform spectral estimation method applied to data from a single hydrophone. Chapman's source spectrum model was used. Reverberation models based on Lambert's law and omnidirectional backscattering theory were compared. Lambert's law was found to be more applicable in the Barents Sea. A statistical analysis was performed on broadband and narrowband hydrophone data showing that reverberation in the Barents Sea possesses Gaussian properties.

14. SUBJECT TERMS			15. NUMBER OF PAGES 80
			16. PRICE CODE

17. SECURITY CLASSIFICATION OF REPORT Unclassified	18. SECURITY CLASSIFICATION OF THIS PAGE Unclassified	19. SECURITY CLASSIFICATION OF ABSTRACT Unclassified	20. LIMITATION OF ABSTRACT UL

NSN 7540-01-280-5500

Standard Form 298 (Rev. 2-89)
Prescribed by ANSI Std. 239-18

Shallow Water
Reverberation
Measurement and Prediction

by

Charles E. Muggleworth
Lieutenant, United States Navy
B.S.E.E., United States Naval Academy, 1987

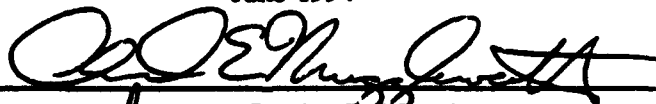Submitted in partial fulfillment
of the requirements for the degrees of

MASTER OF SCIENCE IN ELECTRICAL ENGINEERING
and
MASTER OF SCIENCE IN ENGINEERING ACOUSTICS

from the

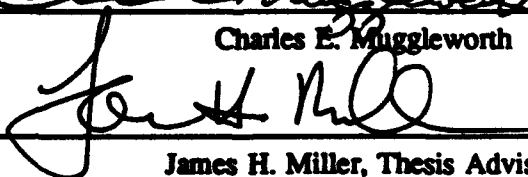NAVAL POSTGRADUATE SCHOOL
June 1994

Author: _____
Charles E. Muggleworth

Approved by: _____
James H. Miller, Thesis Advisor

_____
Ching-Sang Chiu, Thesis Advisor

_____
James V. Sanders, Chairman
Engineering Acoustics Academic Committee

_____
Michael A. Morgan, Chairman
Department of Electrical and Computer Engineering

TABLE OF CONTENTS

ABSTRACT

Low frequency active sonar performance in shallow water is often limited by reverberation. Reverberation modeling in shallow water has been difficult due to the complexity of the multipath acoustic propagation problem inherent in shallow environments. In August 1992, a shallow water, low-frequency reverberation measurement was made in the Barents Sea utilizing explosive "signal, underwater sound" (SUS) charges as sound sources and a 16-element vertical hydrophone array as the receiver. The objectives of this thesis were to analyze the reverberation data from this experiment, compare several theories which have been proposed to model reverberation, and determine the reverberant characteristics of the region. The three-dimensional Hamiltonian Acoustic Ray-tracing Program for the Ocean (HARPO) was used as the primary propagation modeling tool. The temporal signal processing consisted of a short-time Fourier transform spectral estimation method applied to data from a single hydrophone. Chapman's source spectrum model was used. Reverberation models based on Lambert's law and omnidirectional backscattering theory were compared. Lambert's law was found to be more applicable in the Barents Sea. A statistical analysis was performed on broadband and narrowband hydrophone data showing that reverberation in the Barents Sea possesses Gaussian properties.

iii

ACKNOWLEDGEMENTS

I. INTRODUCTION

A. MOTIVATION

As the world political climate continues to shift, the new naval battlefield has been extended into littoral regions (O'Keefe, 1992). Prosecution of a new breed of coastal diesel submarines has become a top priority for ensuring U.S. forces maintain battlespace dominance in these regions. The development of low frequency active acoustic (LFAA) systems by several nations worldwide, including the United States, may provide new, more effective methods by which such forces can be combatted. Such systems represent a double-edged sword, however, because their potential effectiveness in the detection and prosecution of diesel submarines operating in littoral regions implies a threat to the tactical security of U.S. submarines. Hence, performance predictions for LFAA systems have become a priority for the Navy.

The performance of LFAA systems in shallow water is often limited by reverberation from the bottom. Reverberation modeling is a complex task, for it involves nearly every aspect of underwater acoustics research. It incorporates environmental monitoring, propagation modeling, underwater explosion theory, array analysis, and scattering theory into a single field of research. Because the problem is so complex, reverberation modeling has been historically difficult due to the lack of adequate

1

processing power. Hence, even though the need for accurate predictions has existed for many years, only recently has it been possible to adequately model the problem.

In the past, much research effort has been expended in the study of reverberation in deep water. Most of the experiments have involved relatively simple propagation and scattering models (McCammon, 1993). They have mainly used point sources and single hydrophone receivers to analyze energy which traveled on a single path to a scatterer and then returned on that same path. This lessened the computational load significantly, but limited the range for which the analysis was accurate. Nonetheless, in deep water, these relatively simple models were adequate to produce relatively accurate performance predictions of sonar systems.

In shallow water, due to the multipath acoustic propagation taking place, such models were not adequate. Hence, a more accurate, and necessarily more complicated modeling technique was needed. This need motivated the inclusion of a low frequency reverberation study as part of the Barents Sea Polar Front Experiment (BSPFEX). In this experiment, a vertical array and explosive "signal, underwater sound" (SUS) charges were utilized to conduct low frequency reverberation measurements. These measurements then provided baseline data which have been used in this thesis to test the validity of reverberation prediction models.

The experiment also provided a valuable opportunity to investigate the statistical properties of reverberation in the Barents Sea. In a shallow water environment with a rigid bottom such as the BSPFEX experiment area, the highly multipath nature of acoustic propagation creates a reverberant signal which is a combination of many random

2

processes, each of which may or may not be Gaussian. By the central limit theorem, however, the sum of these signals arriving at a single hydrophone should possess a normal Gaussian distribution. This hypothesis was examined as part of this BSPFEX data analysis for both narrowband and broadband signals.

B. OBJECTIVES AND APPROACH

The main thrusts of this thesis can be summed up in three objectives. The first was to examine two commonly used laws for reverberation prediction as applied to the Barents Sea, namely Lambert's law and omnidirectional scattering. The second objective was to estimate the environmentally-dependent reverberation model parameter μ for the Barents Sea and to determine its frequency dependence. The third objective was to perform a statistical analysis of the BSPFEX data to determine if the characteristics of reverberation in the region did in fact possess Gaussian properties.

Considering the oceanographic data available from unclassified sources and the computing resources on hand, the following methods/models were used for theoretical predictions and data analysis in this thesis. Narrowband data analysis was performed using short-time Fourier transforms for all power spectral density estimates. Statistical analysis was performed on broadband and narrowband data using normalized data segments and histograms. Propagation modeling was performed utilizing ray theory as implemented in the Hamiltonian Acoustic Ray-tracing Program for the Ocean (HARPO), with post-processing performed on the HARPO output to determine the effects of spreading and boundary interactions. Geometric effects were accounted for using a ray-

3

tube spreading algorithm. Boundary interactions were accounted for using the Rayleigh reflection coefficient and Eckart rough surface scattering function. The propagation due to a point source was approximated using four ray launch azimuths ("4 x 2D" estimate). Backscattering functions developed by Lambert, Tolstoy and Clay, and McCammon were investigated. A SUS source model developed by Chapman (1988) was used. Finally, the propagation model, backscattering function, and source model were combined to produce a narrowband reverberation envelope prediction for the Barents Sea. By comparing theoretical predictions for the Barents Sea with the experimental measurements, the validity of each reverberation theory was tested.

The most significant choice of the the models/methods listed above was that of the propagation model, for it had the greatest effect on the level of the predicted signal and it determined which models or methods were appropriate for boundary interactions and scattering. All routines developed for this thesis were programmed in the MATLAB® environment and implemented on an HP 9000 series 735 computer (TAC 3), a general purpose UNIX based machine.

C.   OVERVIEW OF THESIS

The approach described above is summarized in Figure 1.1. Environmental data were gathered from unclassified sources, including bathymetric and geologic data from recent publications and sound speed field data determined during the BSPFEX. HARPO was used to trace rays on several azimuths from the array location in order to estimate the three-dimensional propagation effects which determine the transmission paths between

4

were compared to determine the validity of the scattering functions used. The statistical analysis of the BSPFEX data was performed as previously described and compared with a normal Gaussian distribution to verify its statistical properties agreed.

In Chapter II, details of the reverberation experiment in the BSPFEX are presented. The discussion includes a brief discussion of oceanographic and geologic features of the Barents Sea, a description of the SUS charges used as sound sources, and the construction and operation of the vertical array. This is followed in Chapter III with a discussion of reverberation theory, both in general terms and specific theories which have been developed. Theories to be presented include Lambert's Law, Tolstoy and Clay's low frequency scattering function, and McCammon's low frequency, low grazing angle backscattering strength model. Chapter IV presents a method for predicting bottom reverberation using HARPO, a source model, and a backscattering strength model. It also presents the results of the BSPFEX and compares them to the predicted levels. It ends with an analysis of the statistical properties of the reverberation measured during the experiment. Finally, Chapter V summarizes the work completed and discusses lessons learned. Advice regarding future work to refine the present study will be provided.

our point source (SUS), bottom locations, and a hydrophone. A SUS source spectrum model from recent research was used as a second input to the reverberation prediction. The last factor needed was the bottom scattering strength function $S_b(f,\theta_o,\theta)$. Scattering functions suggested by Lambert, Tolstoy and Clay, and McCammon were considered. With these inputs, the reverberation level present at the array was predicted.
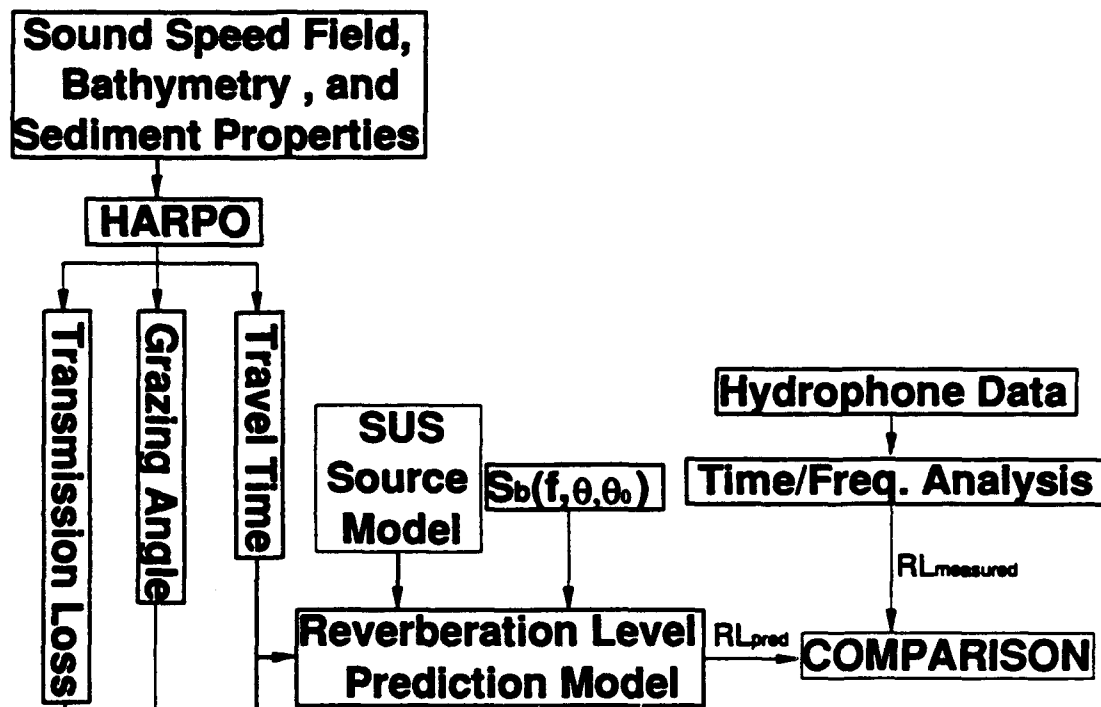
Figure 1.1: Reverberation level measurement and prediction flowchart.

The measurement portion of the problem was addressed in a somewhat more straightforward manner. A spectral analysis subroutine was applied to the hydrophone data to produce a time series of reverberation level at specific frequencies. Frequencies of 50, 100, 200, and 400 Hz were considered in this thesis. These frequencies have no special significance (i.e. to an existing LFAA system), other than the fact that they cover the array's 50 to 500 Hz bandwidth in octave steps. The measured and predicted levels

II. BARENTS SEA EXPERIMENT

A. EXPERIMENT OBJECTIVES

The Barents Sea Polar Front Experiment (BSPFEX) was conducted in August of 1992. The experiment was a joint effort between the Naval Postgraduate School (NPS), Woods Hole Oceanographic Institute (WHOI), and the Science Applications International Corporation (SAIC). The principal investigators for the experiment were Professors Ching-Sang Chiu, James H. Miller, and Robert Bourke from NPS, Dr. James F. Lynch from WHOI, and Dr. Robin Muench from SAIC. The principal engineers for the development and deployment of the vertical hydrophone array system were Mr. Keith von der Heydt and Mr. John Kemp from WHOI. The objectives of this experiment as outlined by the Barents Sea Polar Front Group (1992) were:

1. Provide a detailed physical description of the polar front.

2. Enhance the understanding of dynamics of the front, including frontogenesis and its influence on regional oceanographic processes.

3. Assess the ability of acoustic tomography to define frontal and associated mesoscale features.

4. Provide improved documentation of shallow water acoustic propagation in this region and the effect of the environment on acoustic Anti-Submarine Warfare (ASW) operations.
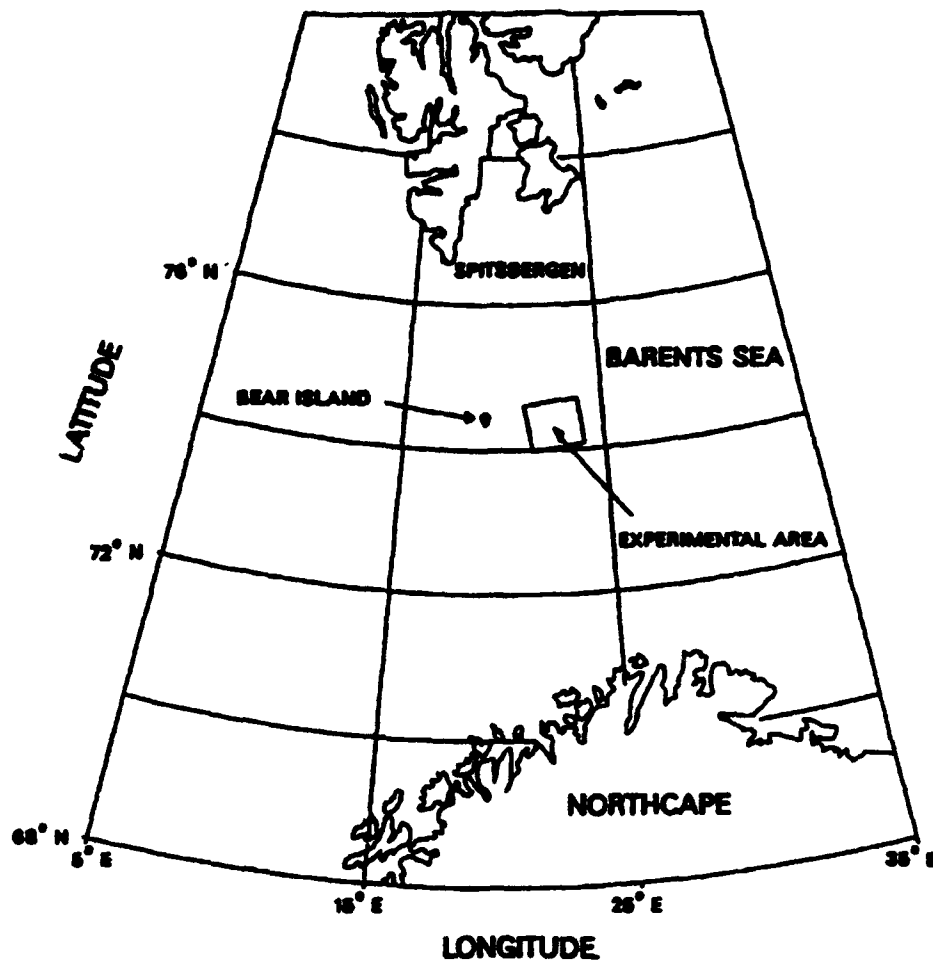
Figure 2.1: The Barents Sea.

The reverberation experiment was designed to meet part of the fourth goal by studying low frequency sound propagation and scattering in shallow water. (McLaughlin, 1993)

B.   EXPERIMENT LOCATION

The experiment was performed in the Barents Sea 100 km east of Bear Island, as shown in Figure 2.1. The Barents Sea forms an epicontinental sea (1.3 million km^2), bounded by the Arctic Ocean to the north, the Svalbard archipelago and the Norwegian-

8
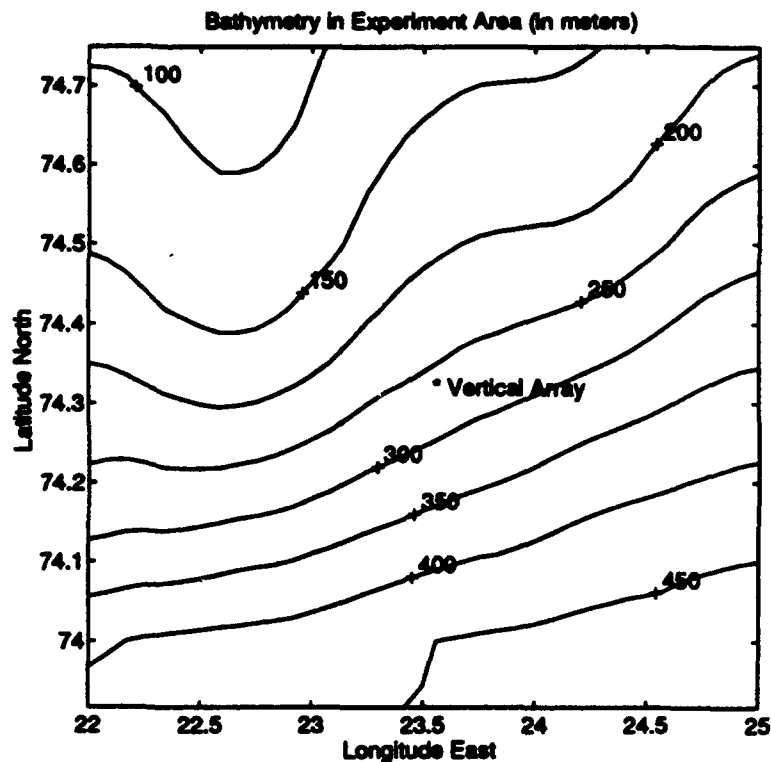
Figure 2.2: Bathymetry in the BSPFEX area.

Greenland sea to the west, the Fennoscandian shield in the south and Franz Josef Land and Novaya Zemlya to the east. It is characterized by northeast-southwest trending basins 300 to 500 meters in depth, with an average depth of 230 meters over the entire region. It is thus significantly deeper than most of the present day high Arctic shallow shelves outside North America, Northern Europe and Northern Asia (which are generally 10 to 60 meters deep). The greater depth is most likely a response to repeated glaciations in the Late Cenozoic, leaving only a thin sediment cover above the Mesozoic and Paleozoic bedrock (typically 5 to 15 meters thick) (Norsk Polarinstitutt, 1987).

The majority of the Barents Sea is covered with a thin sediment layer, though large sediment distributions are present in water depths exceeding 300 meters in the western part of the major troughs Bjørnøyrenna and Storfjordrenna and exceed 500 meters in thickness near the shelf edge. In the experiment area, the sediment thickness varies from nearly 0 msec (exposed bedrock) in the northern portion to approximately 50 msec near the southern extent of the area. The majority of the sediment is composed of stiff pebbly mud, till and/or glaciomarine deposits overrun and reworked by glacial activity (Norsk Polarinstitutt, 1987).
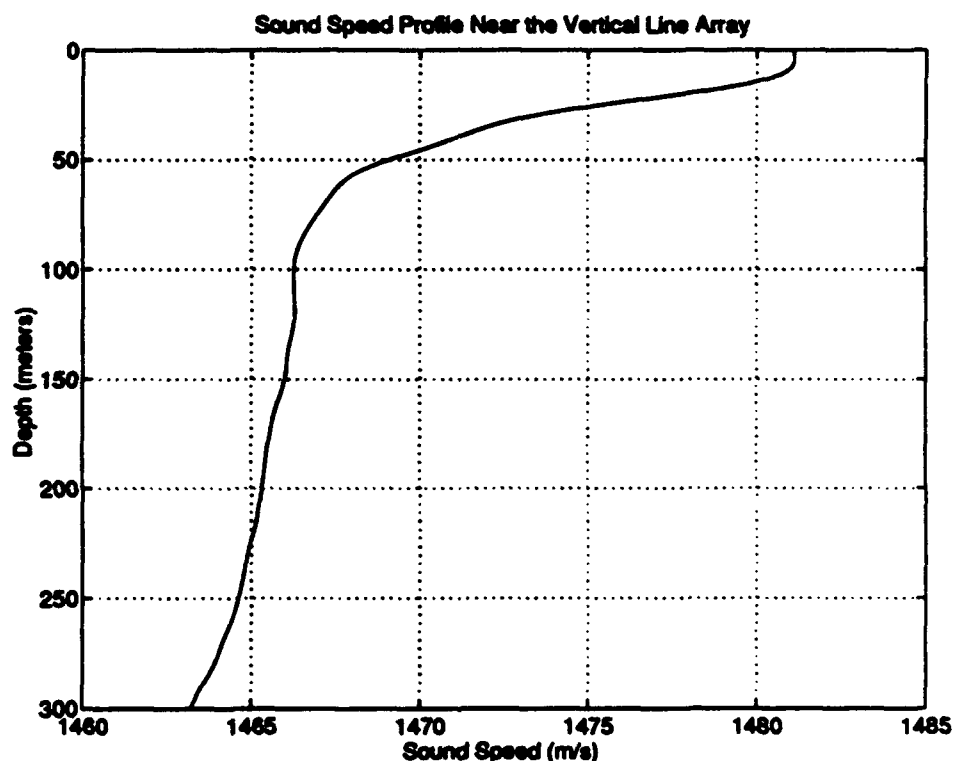
Figure 2.3: Sound speed profile near the vertical line array.

Near the experiment area, the oceanography is dominated by the Barents Sea Polar Front. It is a stable feature which is caused by circulation in the region (Emblidge, 1991)

10

and which passes directly through the experiment area approximately 5 km north of the receiving array. The physical oceanography of the region plays a large role in controlling sound propagation. The bottom, as previously described, is rough in some areas and consists of a thin sediment overlying hard rock. The bathymetry (Figure 2.2) and sound speed are highly range dependent. The shallow water and generally downward refracting sound velocity profile cause many surface and bottom interactions in the acoustic propagation.

The sound speed field was observed to vary significantly with range. The sound speed profile measured at the vertical line array is shown in Figure 2.3 and is a typical Barents Sea profile south of the front for the summer. The sound speed gradient is basically negative from surface to bottom with a shallow mixed layer region. The negative gradient tends to bend rays toward the bottom, enhancing the region's already strong bottom reverberation characteristics and minimizing surface reverberant effects.

C. EQUIPMENT DESCRIPTION

The locations for the vertical line array and the SUS charges which were processed are shown in Figure 2.4 and are listed in Table 2.1. A description of each follows.

1. SUS Charges

A total of 24 SUS charges were expended during the experiment. Eighteen of the charges were delivered by a P-3 Orion aircraft which overflew the data recording ship on two courses, 242°T and 351°T, dropping 9 SUS charges on each run. The SUS charges dropped by the P-3 were U.S. Navy Mark 64-0 exercise communication SUS,

11
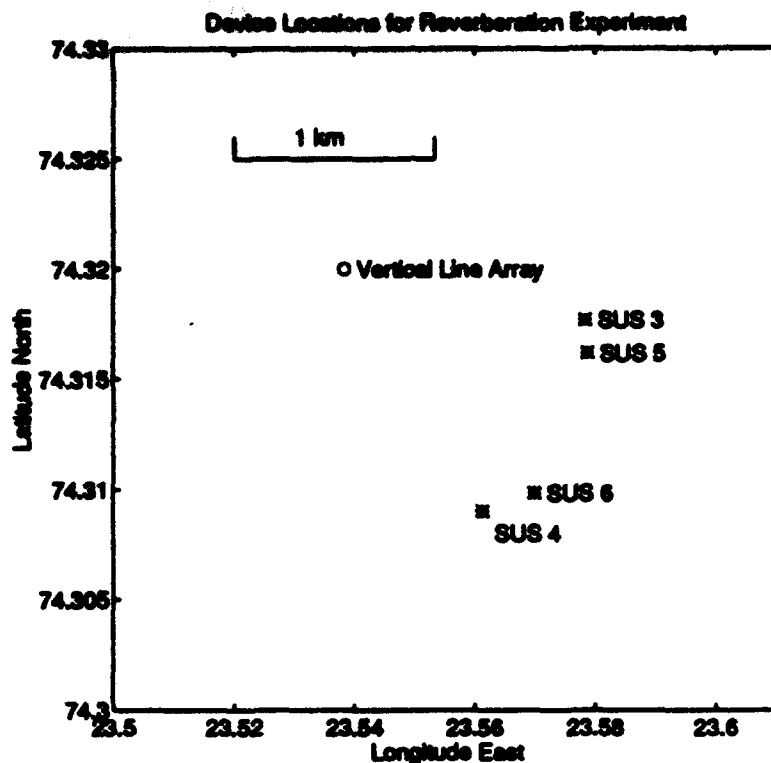
Figure 2.4: Device locations for reverberation experiment.

which contain a 1.1 lb (0.50 kg) TNT main charge and were set to explode at 60 ft (18 meters). The charges have a nominal broadband source level of 263 dB re 1μPa @ 1 meter (U.S. Navy, 1989). All of the air-dropped charges exploded and were recorded, but the 60 foot detonation depth placed the charges well within the mixed layer. Although they were easily heard by the array, the reverberation created by the charges was minimal and the high propagation loss between the detonation points and the array severely attenuated the signal. Hence, the recordings of the air-dropped SUS are of little use for this particular research.

The remaining six charges were thrown by hand off the back of the recording ship. One of the six was a dud, and one was not recorded. The ship-dropped SUS

TABLE 2.1: DEVICE LOCATIONS

Device	Latitude	Longitude	Distance to Array
Vertical Line Array	74° 19.1994'N	23° 32.2957'E	N/A
SUS 3	74° 19.06'N	23° 34.70'E	1232 meters
SUS 4	74° 18.54'N	23° 33.68'E	1405 meters
SUS 5	74° 18.97'N	23° 34.72'E	1287 meters
SUS 6	74° 18.59'N	23° 34.20'E	1479 meters

charges used were U.S. Navy Mark 82 special purpose SUS, which contain a 1.8 lb (0.82 kg) TNT main charge and are set to explode at a depth of 300 ft (91.4 meters). The charges have a nominal broadband source level of 274 dB re 1µPa @ 1 meter (U.S. Navy, 1989). They were dropped at an average range of 1350 meters from the array and produced a reverberation signal which is distinguishable above the background noise level for approximately 50 seconds.

Qualitatively speaking, Mk 82 SUS provide an impulsive signal which, although non-linear in the immediate vicinity of the source, serves as a very close estimate of a point source with an impulse-like pressure signature. A time series of one such explosion is shown in Figure 2.5. As noted in the following paragraphs, the signal would be even more impulsive in appearance if it had not been for non-linearities in the receiving array. A more complete discussion of underwater explosion theory is discussed in Chapter III, Reverberation Theory.
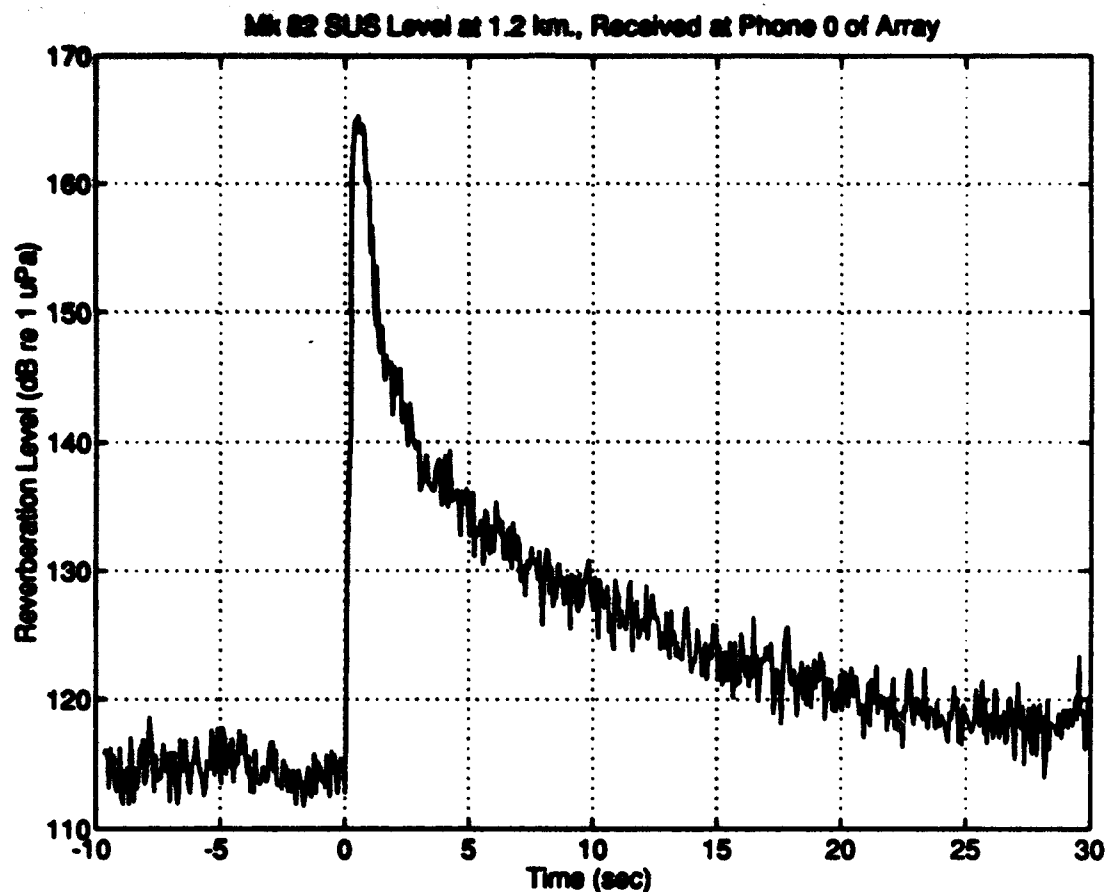
Figure 2.5: Received direct blast and reverberation for SUS 3.

2. Vertical Line Array

The vertical line array is shown in Figure 2.6. The array consisted of 16 hydrophones spaced 10 meters apart. The hydrophones had a nominal sensitivity of -160 dB re V/μPa. The mooring was designed to acoustically decouple the surface buoy from the array and hence minimize the effect of surface waves on mooring motion. The surface buoy contained an RF Ethernet system which transmitted the digitized data to the ship (Von der Heydt, et al., 1992). On the ship the data was stored on tape for later analysis.

14
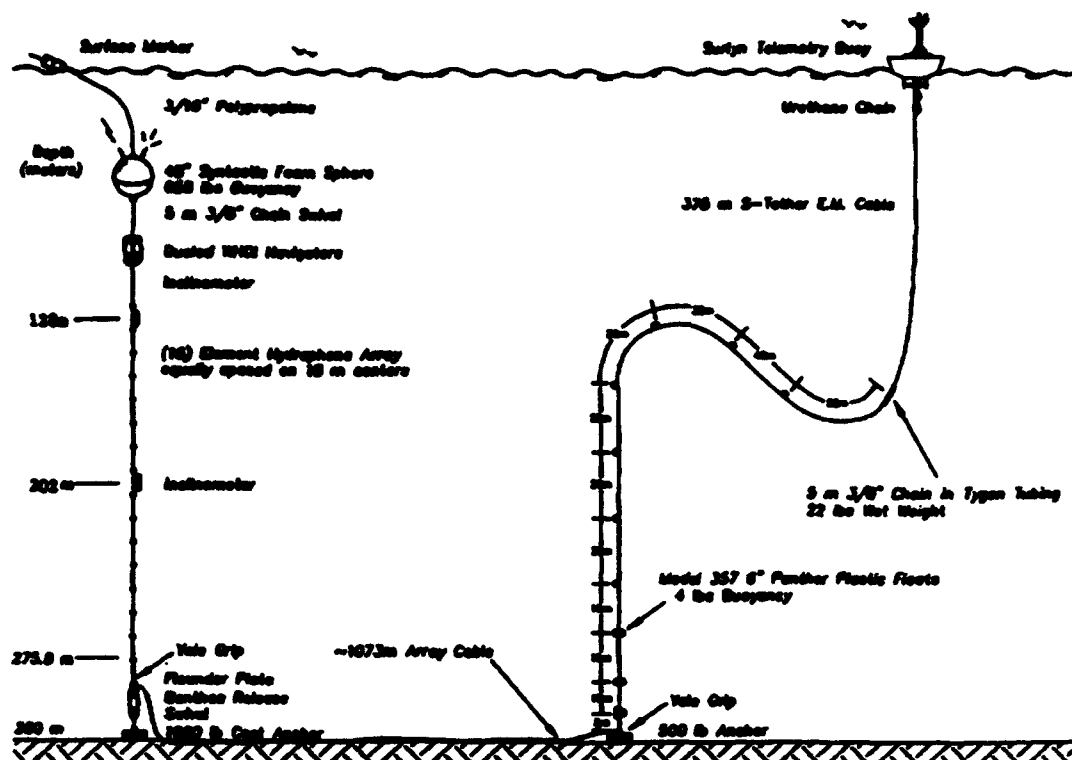
Figure 2.6: Vertical line array and RF Ethernet buoy. (Von der Heydt, et al., 1992)

In the tomography experiment, the sign (+/-) of the signal made little difference, since the only significant data was the travel time of the signals. In the reverberation experiment, it was found that the received signals were consistently 180° out of phase with theory due to the details of the data acquisition system. This shows up most vividly in the initial blast waveform, which should be initially an overpressure in the ground wave, then the waterborne shock wave, again positive-going, followed by several positive-going bubble pulses. After the initial arrivals, arrivals from other multipaths, including surface reflections (which do undergo a 180° phase shift and hence would be initially negative-going) come in but are complicated by the bubble pulses of the previous arrivals. The corrected signal is shown in Figure 2.7. In all data analysis,

15
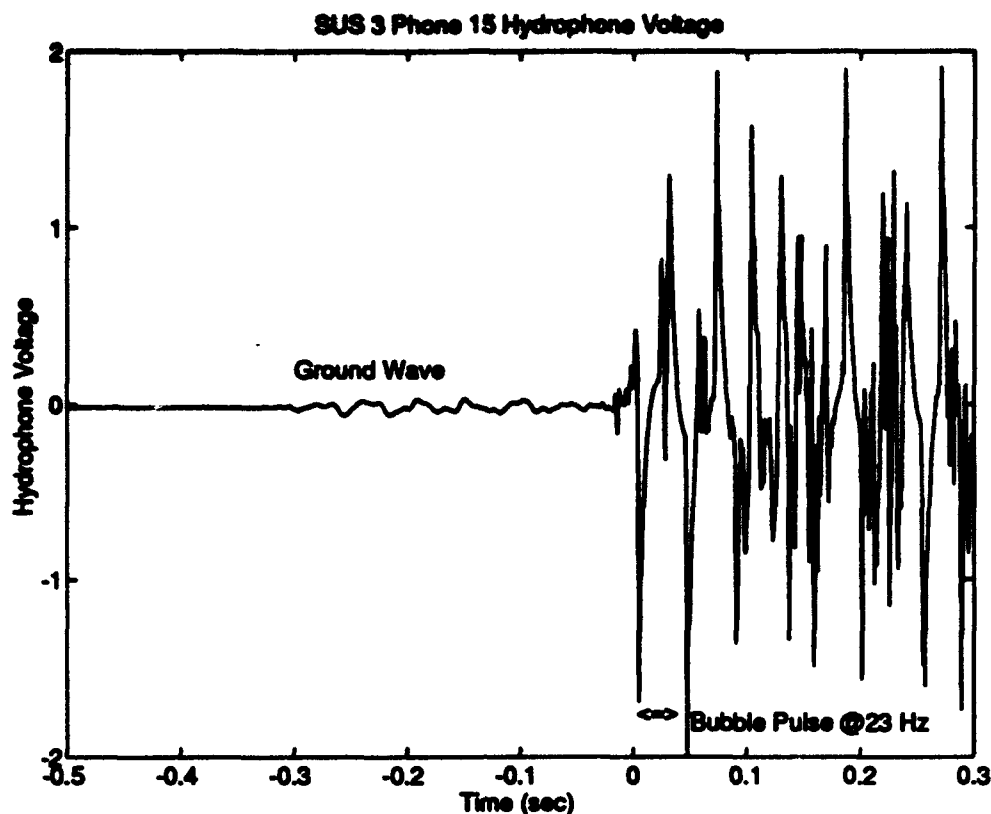
Figure 2.7: Initial received waveform from Mk 82 SUS.

the polarity of the received signal will be reversed in order to account for this feature.

An additional undocumented feature of the vertical line array was discovered during analysis of the SUS explosion time series. Either the hydrophones on the array or the analog-to-digital (A/D) converter in the buoy showed a non-linear response at levels exceeding ~160 dB (1 volt), with the signal entirely clipped above 165 dB (1.8 volts). Figure 2.8 illustrates this clearly during the first half second of the received blast. The signal should have been a sharp increase to a peak (at ~195 dB), followed by a near linear decrease in amplitude (in decibels). This would correspond to an exponential decrease in pressure with time. Instead, the signal remains at the maximum phone output level until the initial shock wave and first bubble pulses pass. The A/D converter had

16
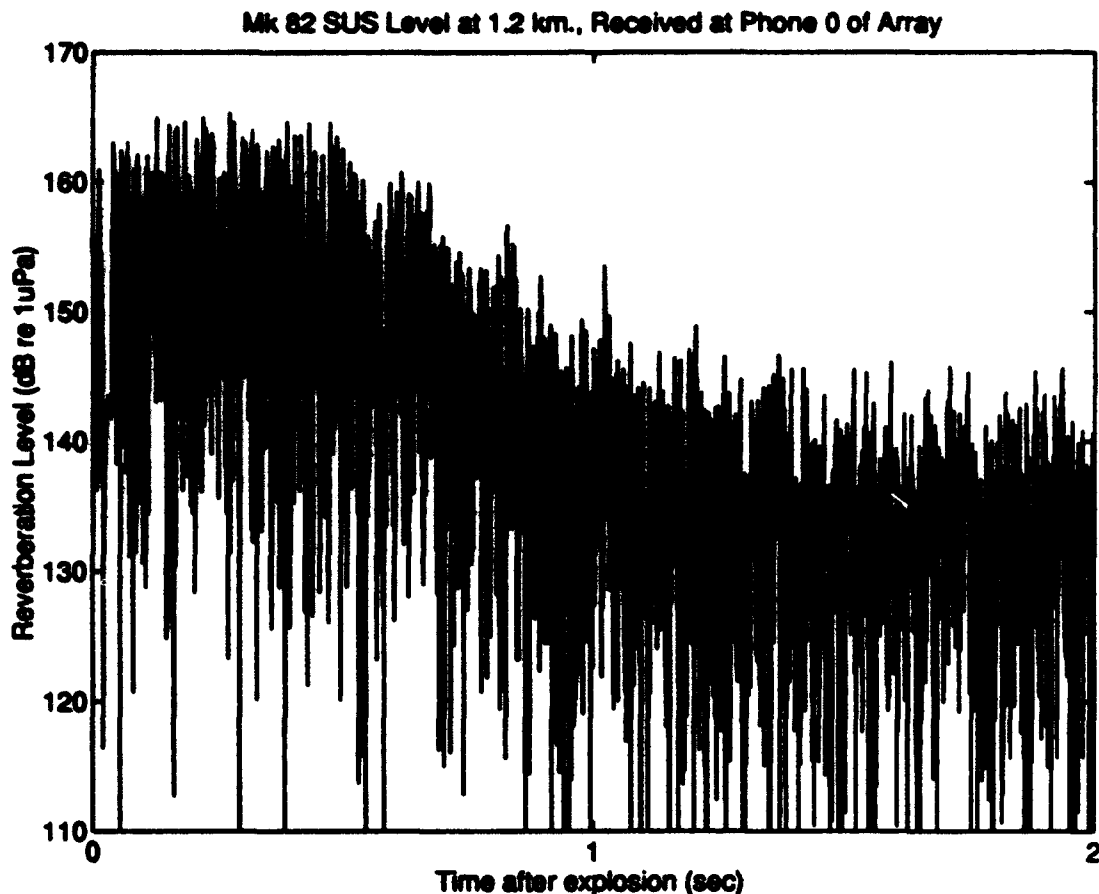
Figure 2.8: Reverberation level plot showing clipping of hydrophone output.

been specifically designed to show a linear response over -5 volts to 5 volts hydrophone output. Therefore, the phones themselves were likely the source of the non-linear behavior. To be conservative, it is assumed that the phones display a non-linear amplitude response over 150 dB re 1 uPa, as is illustrated graphically in Figure 2.9.

The implication of this on the reverberation experiment is that approximately the first second of the SUS explosion data is unusable. This is unfortunate, since any time-domain methods of reverberation require a time series as the input signal to the

17

reverberation equation. Because of this, spectrum levels of SUS charges from recent research have been used in all data analysis and prediction routines.
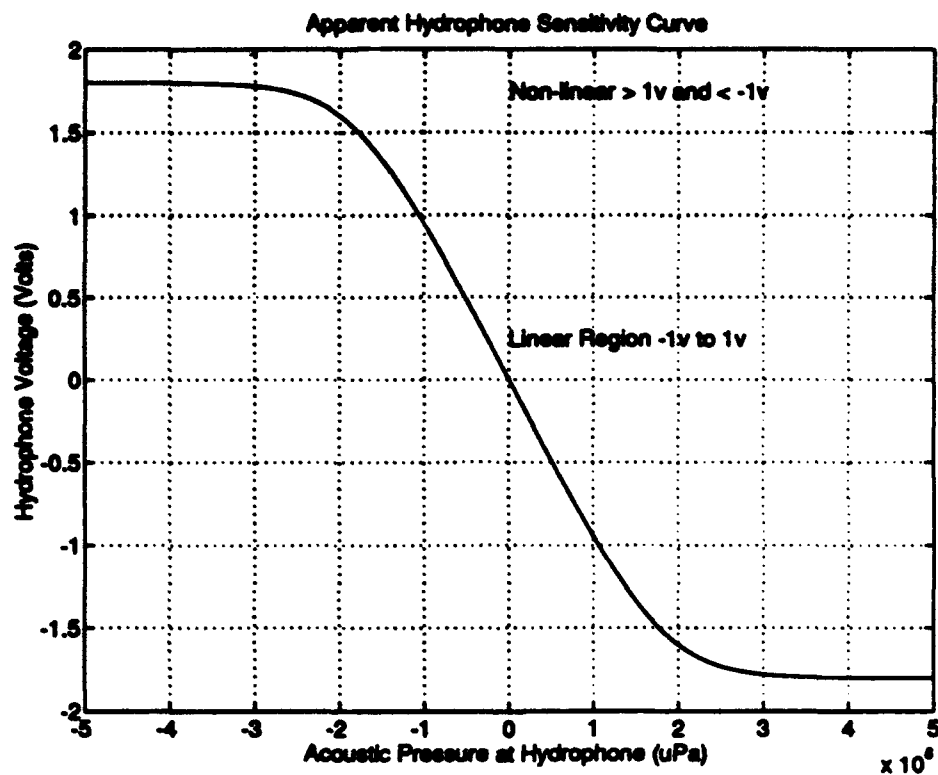
Figure 2.9: Apparent hydrophone response curve.

III. REVERBERATION THEORY

A. GENERAL REVERBERATION THEORY

Any discontinuity in the physical properties of a medium tend to intercept and reradiate a portion of the acoustic energy incident upon them (Urick, 1983). This reradiation of energy is called *scattering*, and the sum total of scattering from all scatterers in the medium to a receiver is called *reverberation*. These discontinuities can be due to any type of inhomogeneity present in the sea. Particles of inhomogeneous material (dust, fish, bubbles, etc...), the sea surface, the bottom, and changes in sound velocity in the medium away from a perfect isovelocity structure (vertical or horizontal effects) all contribute as scatterers.

Reverberation can be generally categorized into two broad areas: Volume and surface. *Volume reverberation* is due to energy which has undergone scattering with some inhomgeneity which is suspended in the water volume and then has propagated back to the desired receiver location. Examples of scatterers which contribute to volume reverberation include marine life, suspended sediment particles, and bubbles. *Surface reverberation* is due to energy which has undergone scattering with some inhomogeneity in the form of a flat plane. The two most commonly considered types are sea-surface reverberation and bottom reverberation. Several types of volume reverberation, however, can be effectively modeled with an equivalent surface reverberant layer. Perhaps the most

19

well-known example of this method is the so-called deep scattering layer, which is in fact a thick layer of marine life which tends to vary in depth depending on the time of day and the season. Due to its plane-like structure, it is typically more efficient and equally accurate to model its effect using a surface of equivalent scattering strength located in the proximity of the layer volume.

Due to the statistical nature of the large number of scatterers contributing to the total reverberation level at any one time, reverberation is usually discussed in decibels referenced to 1 µPascal (dB re 1µPa) instead of describing it as a time series in terms of pressure for a particular medium. As such, the most general form of the bistatic reverberation equation is:

$$RL = SL - TL_{source-scatterer} - TL_{scatterer-receiver} + TS_R \qquad (3.1)$$

SL is the *source level* of the projector used for the active sonar system and is typically given in decibels referenced to 1 µPascal at one meter (dB re 1µPa @ 1 m). For sources which are beamformed, this term may be different depending on the angle from which the energy leaves the source. SL may be given as the total level over a band of frequencies or as a narrowband power spectral density referenced to a 1 Hertz bandwidth (units of dB re 1 µPa²/Hz @ 1 m). The two TL terms represent the *transmission* (propagation) *loss* from the source to the scattering inhomogeneity (scatterer) and from the scatterer to the intended receiver of the sonar. Energy traveling from the source to the scatterer on one "path" will, in most cases, be scattered back to the receiver along many paths connecting the scatterer and the receiver. For this reason, the propagation

20

modeling which is used both in prediction and data analysis methods can be the most significant choice that is made in the reverberation modeling process.

The last term, TS_R, (reverberant target strength) is the ratio (usually given in decibels) of incident power arriving at the scatterer on one path to the power which is retransmitted along a return path to the receiver. This term is dependent on both the characteristics of the volume or surface causing the scattering and the total area or volume of the scatterer. There are two possible ways in which such interactions may be predicted. The first, *discrete backscatter prediction* (Medwin, 1981, Clay et al., 1977, and Dyer et al., 1993), involves a detailed knowledge of the scattering surface. Each scatterer ("wedge", "plane strip", or "facet", respectively) must be identified and its effect on incoming energy quantized in order to effectively predict the resulting backscattered field. Every interaction of incoming energy in a given propagation mechanism (eigenray or mode) produces an impulse in the backscattered field which is both weighted by a magnitude and phase term and shifted to a time which is the sum of the travel times from the source to the scatterer, and back to the receiver. This method is analagous to estimating the impulse response of the ocean as if it were a linear, time-invariant filter (Ziomek,1993). The total output reverberation signal is thus determined by a convolution of the input signal (in the time domain) with the impulse response (also in the time domain). As indicated by the discussion, these methods require such precise knowledge of the ocean environment, which is in fact time-varying, as to prohibit accurate prediction. The distinct advantage of this approach, however, is that it produces a signal estimate which is corrected for phase differences due to propagation and scattering, and hence may

21

show finer detail (higher resolution) than do the "envelope" methods discussed below. Methods which employ discrete backscatter prediction have been developed by Medwin (using Biot and Tolstoy's "wedge" theory, 1981), Clay, et al. (using "plane strips", 1977), and Dyer, et al. (using "facets", 1993).

The second method, reverberation *envelope prediction*, entails estimating the *scattering strength* (S_V or S_A) of the surface causing the reverberation depending on the angle or wave number of the incoming and outgoing energy and the type of surface and/or its estimated roughness. A great deal of research effort has been expended to determine scattering strength empirically for every area in the world over a wide range of frequencies. S_V and S_A are given in decibels per unit volume or area (S_V is given in decibels referenced to 1 meter^3 (dB re m^3), S_A in decibels referenced to 1 meter^2 (dB re m^2)). They are in turn multiplied by the volume or area of the scatterer (by adding 10 *log*(Volume) or 10 *log*(Area) in decibels) to give the reverberant target strength TS_R of the entire scatterer. Only the amplitude level (i.e. not the phase) of the reverberant signal is predicted, hence the name envelope prediction. The equations which generate the reverberant target strength are thus:

$$TS_R = S_V + 10 \ \log(Volume)$$
$$= S_A + 10 \ \log(Area) \tag{3.2}$$

In the BSPFEX, the frequencies of concern are determined by the bandwidth of our receiving array, 50 to 500 Hz. In this frequency range the effects of volume reverberation can be assumed negligible after 1 second following the source impulse (NRL 8721, 1991).

22

For reasons discussed at length in Chapter II, the first second of data will not be analyzed. Hence, volume reverberation is not a concern.

This thesis will be mainly concerned with surface reverberation caused by the sea bottom, since the majority of the reverberation in the BSPFEX is assumed to be due to bottom backscatter. This assumption is based on the oceanography in the Barents Sea and the frequencies which are under investigation and the Barents Sea environment. The effect due to the oceanography stems from the fact that the sound speed profiles in the Barents Sea are generally downward refracting with a strong mixed layer, both of which minimize sea surface reverberation and enhance bottom reverberation.

In general, for a surface to be effective at reradiating a particular frequency of sound, it must have features whose size are on the order of a wavelength of sound at that frequency. For example, a sea surface with rms waveheight of 0.5 meter will be an effective scatterer for 10 KHz sound, but a weak scatterer at best for 100 Hz sound. Since the seas were relatively calm during the experiment (less than 0.1 meter rms wave height), surface backscatter can be assumed negligible compared to the effect of the bottom. Experimental data measured by Chapman and Harris support this assumption at a frequency of 500 Hz, placing the surface backscattering strength an order of magnitude lower than our bottom backscattering strength, with the trend serving to minimize the effect of surface reverberation further at lower frequencies (Urick, 1983).

An additional effect of the bottom is *subbottom scattering*, the reradiation or reflection of energy from inhomogeneities below the water/sediment interface. This effect can also be described as bottom volume scattering. Subbottom reverberation is not a

23

concern in the Barents Sea, however, due to the extremely thin sediment layer described in Chapter II and the "fast" rock bottom immediately below the sediment.
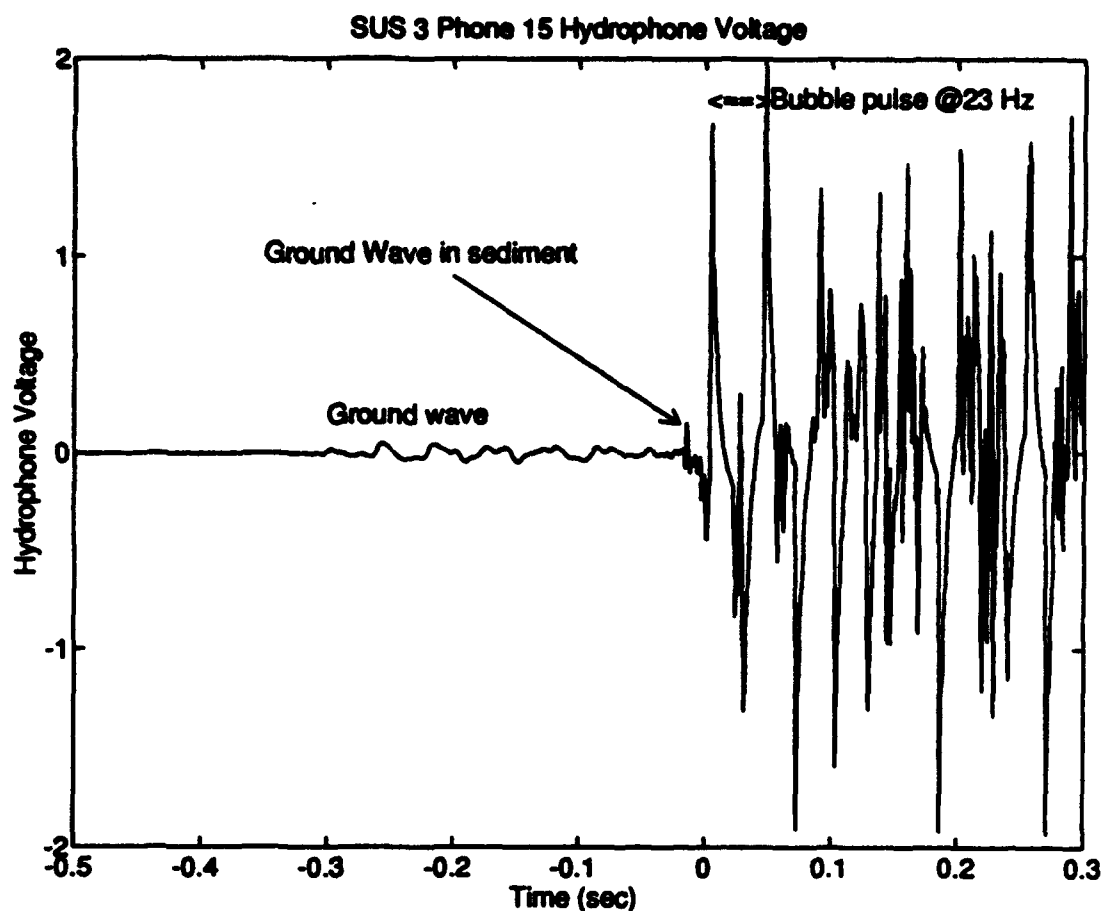
Figure 3.1: SUS 3 ground wave and waterborne arrivals.

To verify this, the speed of sound in the bottom can be calculated using the SUS data. At the leading edge of the received signal is the *ground wave*, energy which has entered the bottom (at the critical angle for the least time path), propagated through the bottom to the array, and then reentered the water column (again at the critical angle) to be received at the array. The ground wave and waterborne arrivals for one of the SUS charges is shown in Figure 3.1. The process by which the difference in travel times is

used is displayed graphically in Figure 3.2. The speed of sound was found to be greater than 3000 m/sec in the bottom, verifying that the subbottom scattering is insignificant.
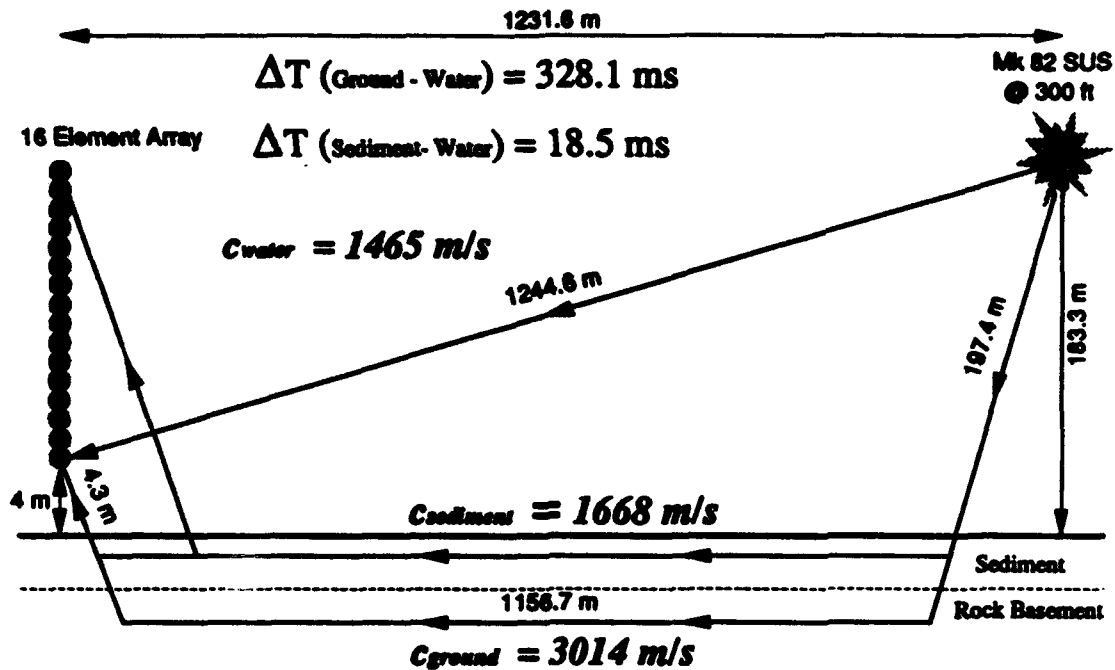
Figure 3.2: Use of ground wave to determine sound speed in the bottom.

An additional effect is shown in Figure 3.1 immediately before the waterborne energy arrives. The small positive-going spike approximately 20 msec. prior to the direct path blast arrival is most likely energy which was trapped in the thin sediment layer. Using the travel time difference between it and the waterborne energy, the sound speed of the sediment layer is calculated as $c_{sediment} = 1668$ m/s. This number can then be used along with the frequency content of the trapped energy to determine the sediment thickness. The dominant frequency present in the energy trapped within the sediment "waveguide" is 286 Hz (accounting for the energy still propagating in the rock basement

ground wave). This yields a sediment thickness measurement of 5 meters, which is consistent with tabulated data for the region. The significance of the sediment sound speed and thickness lay in the fact that the energy trapped within the sediment layer is minimal, and the sound speed of the sediment is such that the layer is almost acoustically transparent.

Hence, with sea-surface reverberation and volume reverberation (both in the water column and in the bottom) insignificant with respect to bottom reverberation, a discussion of bottom backscattering theory is warranted.

B. BOTTOM SCATTERING THEORY

The bottom is an effective reflector and scatterer of sound and acts to redistribute a portion of the sound incident upon it back into the ocean above it (Urick, 1983). This redistribution of energy is illustrated in Figure 3.3, which shows the effective "beam pattern" of the sea bottom for reradiating incident sound energy. Four cases are shown, illustrating the four general cases which occur in bottom scattering. The first and second general cases (cases (a) and (b)) describe bottoms which have a high *impedance contrast* with the water volume, where the acoustic impedance of a medium is defined as the product of the medium's density ρ and sound speed c. Any sufficiently hard bottom fits this definition, be it rocky or hard sand. Note that almost all of the incident energy is redistributed in the water volume above, with roughness determining the relative strength of the specular reflection. Cases (c) and (d) show the scattered field for bottoms which have low impedance contrast with the water column. Bottoms of this type are sometimes

26
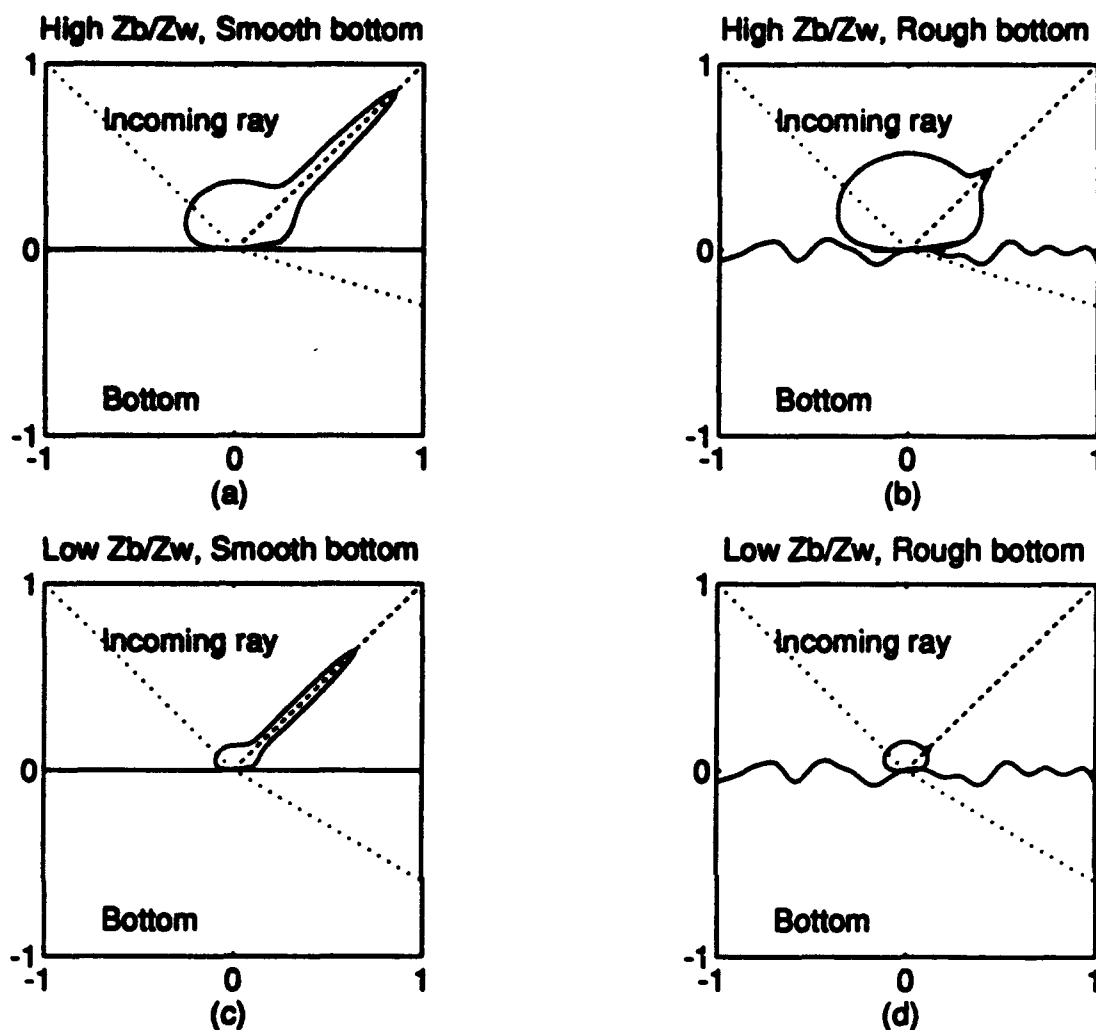
Figure 3.3: Directional patterns of the scattered sound from the bottom for different conditions of roughness and impedance (Z=ρc) contrast. (Urick, 1983)

called *acoustically transparent* in that most energy is propagated into the bottom, leaving relatively little to be distributed back into the water volume above. Examples of these bottoms are soft mud or silty bottoms with a thick sediment layer. Note that bottom roughness is still a dominant factor in the magnitude in both the specular and scattered directions.

This brings up an interesting fact. Although the type of bottom sediment deposits may serve as a first-cut means of classifying bottoms in terms of acoustic backscattering, the roughness of the sea bottom appears to be the dominant factor in determining the backscattering characteristics. Just as wind speed has for many years been used as an indicator of surface roughness and bubble density near the surface, so is the bottom type merely an *indicator* of bottom roughness. (Urick, 1983)

Many attempts to quantize and mathematically model bottom backscattering are documented. Of these, three theories of bottom scattering will be considered (as discussed by McCammon, 1993):

1. Composite Roughness.

2. Lambert's Law.

3. Omnidirectional Scattering.

1. Composite Roughness

The first theory is that of *composite roughness*, which McCammon describes as, "the most rigorous theoretical approach" (McCammon, 1993), since it can be derived theoretically using the Helmholtz integral equation. Composite roughness theory is composed of two types of scattering mechanisms: facet scatter and Bragg scatter.

a. Facet Scatter

For backscatter due to incident angles greater than 70° grazing, and forward scatter due to all incident angles, facet scatter theory is applicable (McCammon, 1993, and Tolstoy, et al., 1987). It assumes that the bottom is composed of "facets" or

small plane-like structures that *only specularly* scatter coherent and incoherent sound energy. Hence, in order for a facet to scatter energy from a given raypath into a scattered path, the facet must be tilted sufficiently to provide a specular reflection. These types of models require information regarding the bottom's rms roughness height and the spatial correlation length of that roughness. Most assume the surface's roughness is Gaussian. McCammon presents a formula for calculating the scattering strength based on the surface slope and rms slope:

$$S_{facet} = 10 \log\left(Ae^{-0.5(\theta_L/\theta_{rms})^2}\right)$$ (3.3)

θ_L is the local surface slope, θ_{rms} is the rms slope and is given by:

$$\theta_{rms} = \frac{\sqrt{2}H_{rms}}{L}$$ (3.4)

where H_{rms} is the rms surface roughness and L is the spatial correlation length. A is a scaling factor which varies depending on the surface composition. This model has been successfully applied in the modeling of forward scatter and has been included in the BISSM2 Modified Bistatic Scattering Strength Model. (McCammon, 1993)

This model appears quite similar to the low-frequency scattering function for a rough surface with an isotropic Gaussian correlation function developed by Tolstoy and Clay (1987). This function only considers the incoherent scattered radiation relative to the incident radiation:

$$S_\gamma = 10\log\left[\left(\frac{2}{\pi}\right)|\Re|^2\, \gamma^2\sigma^2\, f^2(\theta)\, k^2\, (r_0')^2\, e^{-4\gamma^2\sigma^2-2\kappa\sigma r_0'^2}\right] \qquad (3.5)$$

$\Re$ is the Rayleigh reflection coefficient of the surface, and for angles less than critical, has magnitude equal to 1. γ is the vertical wave number difference for the incident and scattered rays and is given by

$$\gamma = -\frac{k}{2}(\cos\theta_1 + \cos\theta_2) \qquad (3.6)$$

where θ_1 and θ_2 are the incident and scattered angles relative to the vertical and k is the wave number given by

$$k = \frac{2\pi f}{c} \qquad (3.7)$$

depending on frequency f in Hertz and speed of sound c in meters per second. σ is the rms roughness of the surface in meters. $f(\theta)$ is also an angle dependent term which, assuming a two dimensional problem, becomes:

$$f(\theta) = \frac{1+\cos\theta_1\cos\theta_2-\sin\theta_1\sin\theta_2}{\cos\theta_1+\cos\theta_2} \qquad (3.8)$$

r_0' is approximately the correlation length r_0 of the bottom, such that

$$\frac{1}{(r_0')^2} = \frac{1}{r_0^2} + \frac{2}{R^2} \qquad (3.9)$$

where R range of the receiver. In the far field, $r_0' \approx r_0$. Finally κ is the horizontal wave number difference, given in the following equation:

$$\kappa = k(\sin\theta_1 - \sin\theta_2) \tag{3.10}$$

Substituting these definitions into the original equation, we see the somewhat more familiar form:

$$S_y = 10 \, \log\left[\left(\frac{1}{2\pi}\right) k^4 \sigma^2 \left[1 + \cos(\theta_1 + \theta_2)\right]^2 r_0^2 \, e^{-2k^2 r_0^2} \right] \tag{3.11}$$

Compared to McCammon's formula for facet scattering strength, we see an exponential term which depends on the incident angle of radiation and the spatial correlation length of the bottom. The A parameter in McCammon's formula appears to be equal to the remainder of the equation. These two equations (3.3 and 3.11) are significant because they were to be used to check whether the backscattering strength model used in the prediction routine is consistent with the approximate bottom roughness in the Barents Sea.

b. Bragg Scatter

Bragg scatter is applicable to low grazing angles, where composite roughness computes scattering based on interactions with resonant components in the roughness of the surface. Hence, for those components (facets) to be significant, they must have spatial wavelengths equal to twice that of the incident sound. This concept of resonances is similar to that seen in diffraction gratings, hence the name Bragg scatter. The input parameters for this model are the surface height power spectrum $W(K)$ at the resonance wavenumber $K = \kappa$ (Eq. 3.10), which can be derived from the surface rms roughness and correlation length, given the surface roughness has a Gaussian distribution. Bragg backscattering strength in two dimensions is given by

$$S_{Bragg} = 10\log\left(\frac{k^4 \, \sin^2(\theta_0) \, \left[\sin(\theta_0)+\sin(\theta_s)\right]^2 \, W(K)}{4\pi K}\right) \qquad (3.12)$$

where the angles θ_0 and θ_s are the grazing angles of the incident and scattered energy, as in Eq. 3.3 (McCammon, 1993). Again, this theory depends on knowledge of the assumed wavenumber dependence of the spectrum W, which in general is not well documented for most of the ocean bottoms on the planet. This model is based solely on a statistical model of the physical structure of the reflecting surface. Hence, effects due to deterministic structures (bottom features), volume scattering effects (subbottom scattering), or refraction (the basis of discrete backscatter models) are not accounted for. As a result, the effective fourth power dependence on the sine of the grazing angle causes S_{Bragg} to be inaccurate (low) below 20°.

2. Lambert's Law

The second theory is Lambert's law of diffuse scattering. As noted by Urick, Lambert's law is, "a type of angular variation which many rough surfaces appear to satisfy for the scattering of both sound and light." (Urick, 1983) Noting the original application of this "law", he continues:

> Although many materials follow Lambert's law closely in scattering light, none does so exactly. Lambert's law applies specifically to the radiation of light by radiant, absorptive materials; the "law" should properly be called Lambert's "rule" for scattering. Nevertheless, it is, as we have seen, a good description of the backscattering of sound by very rough bottoms. (Urick, 1983)

The original application of Lambert's law was to optics, in which it is known as Lambert's cosine law of diffuse reflection. As described by Houstoun (1938), a portion dS of a surface has apparent brightness which varies with the sine of the grazing
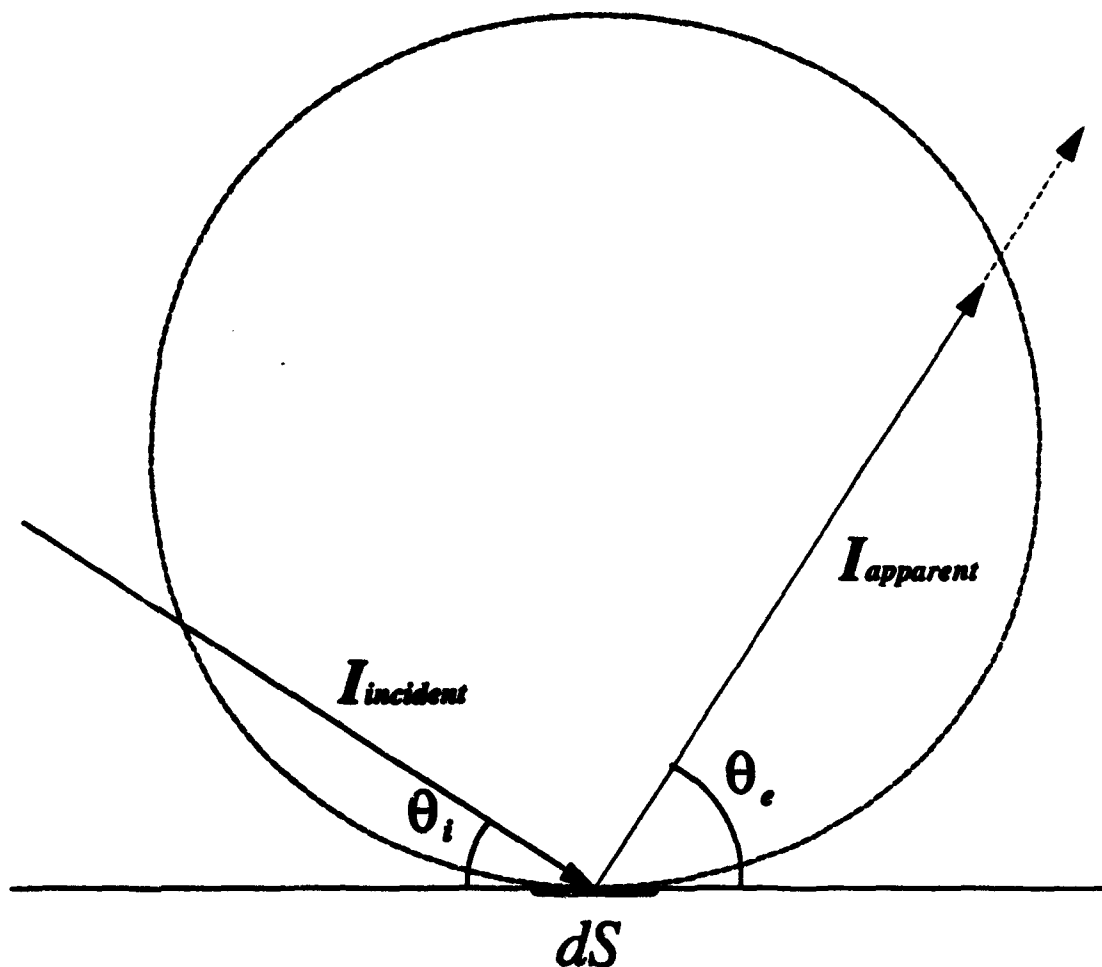
Figure 3.4: Geometry for discussion of Lambert's law of diffuse reflection.

angle of the incident light, but which does not vary with the grazing angle of the reflected light. Specifically,

$$I_{apparent} = \frac{\mu \, I_{incident} \, \sin(\theta_i)}{r^2} \tag{3.13}$$

where, as shown in Figure 3.4, μ is a material dependent constant, $I_{incident}$ is the intensity of the incident light, θ_i is the grazing angle of the incident light and r is the distance between the surface and the observer. $I_{incident} = I \, dS \, \sin(\theta_i)$ is the total light received by

the area dS due to light of intensity I. A practical example of this relationship is a luminous sphere, for example, a red-hot copper sphere heated over a flame. When viewed from a distance, it appears as a disc of uniform brightness over the entire surface when viewed from any angle. Hence, the radiation from an element of the surface making an angle θ_e with that element of the surface must consequently be proportional to $\sin(\theta_e)$ (Houstoun, 1938). The name "cosine law" comes from the fact that in its original development, angle were measured with the normal to the surface, not the grazing angle with the surface itself.

In the application of Lambert's law to acoustics, the scattering strength varies as the product of the sine of the incident and scattered grazing angles times a constant μ that is a function of the material properties of the scattering surface. Thus, scattering strength is given by:

$$S_{Lambert} = 10 \log(\mu \sin\theta_0 \sin\theta_S) = \mu_{dB} + 10 \log(\sin\theta_0 \sin\theta_S) \qquad (3.14)$$

If all of the incident energy were redistributed in the water column, with none lost by transmission into the bottom, it can be shown by integration that $\mu = 1/\pi$, or $10\log(\mu) = \mu_{dB} = -4.97$ dB. In 1961, K. V. Mackenzie reported success using Lambert's law with $\mu_{dB} = -29$ dB to model bottom backscattering in deep water at 530 and 1030 Hz. His conclusions are not viewed as a rigorous theoretical result, but instead a simple geometrical argument which fits the angle dependence of "a lot" of measured bottom backscattering data at moderate grazing angles, specifically $20°$ to $60°$. (Mackenzie, 1961)

34
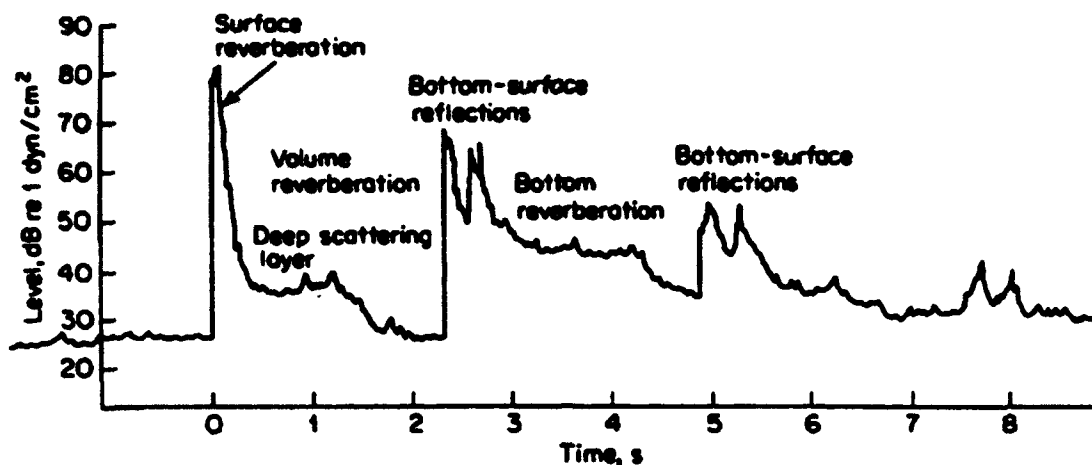
Figure 3.5: Reverberation following a 2 lb. explosive charge detonating at 244 m in water 1980 m deep, as observed with a nearby hydrophone at a depth of 41 m. Filter band 1 to 2 kHz. (Urick, 1983)

The choice of 20° to 60° as limits for the application is not arbitrary. Instead, they result from the geometry of the experiments that were conducted in deep water and the method by which the results were analyzed. As shown in Figure 3.5, reverberation due to the first surface reflections, volume scattering, scattering in the deep scattering layer, and bottom backscatter are separated in time. At approximately 2.4 seconds, the first bottom returns, the so-called *fathometer returns*, come in. At 2.7 seconds the fathometer return from the surface reflection of the explosion arrives at the receiver, followed by a long (~2 second) bottom reverberation return. At 2.7 seconds, the approximate grazing angle of the energy interacting with the bottom is 60°. At 4.8 seconds, after which the next set of bottom-surface reflections arrive at the receiver, the bottom grazing angle of the *direct path* energy (energy which has traveled through the water column only, with no interactions with the surface or bottom) has decreased to

35

approximately 20°. Hence, the limits for the applicability of this *monostatic* reverberation measurement arise naturally from the experimental procedure. The term monostatic is appropriate in this context because the only scattered paths which are significant are those which follow the same grazing angle as the incident energy.

The *bistatic* dependence of Lambert's law has been examined by P. B. Schmidt, again in deep water, in a 1971 paper. He found good agreement with bottom scattering data for incident angles from 3.5° to 78° with scattered return angles from 21° to 84° (McCammon, 1993). The value of μ_{dB} must be set empirically, however, which requires considerable analysis in finding the variation of μ_{dB} with frequency, azimuth angle, and sediment roughness. This theory has been successfully implemented by J. W. Caruthers, et al. in the Modified Bistatic Scattering Strength Model (BISSM2) (McCammon, 1993). They found μ_{dB}= -31.5 dB to best fit their data.

In shallow water, the problem becomes somewhat more complicated. Figure 3.6 shows the return from a 1.8 lb charge used in the BSPFEX. Instead of having clearly separated volume, surface, and bottom returns, they instead all come in simultaneously. The implications of this are two-fold. First, the *dominant* scattering mechanism must be used to predict the reverberation level (in this case, bottom reverberation). Second, the problem is truly bistatic in nature, since the travel time difference between direct path rays and rays which have multiple interactions with the surface and bottom are small, on the order of the decay time of the *bubble pulse* of the explosion (see Section C for a discussion of the bubble pulse and other underwater explosion phenomena). As a result, for each bottom interaction, there are multiple scattered angles which *significantly*
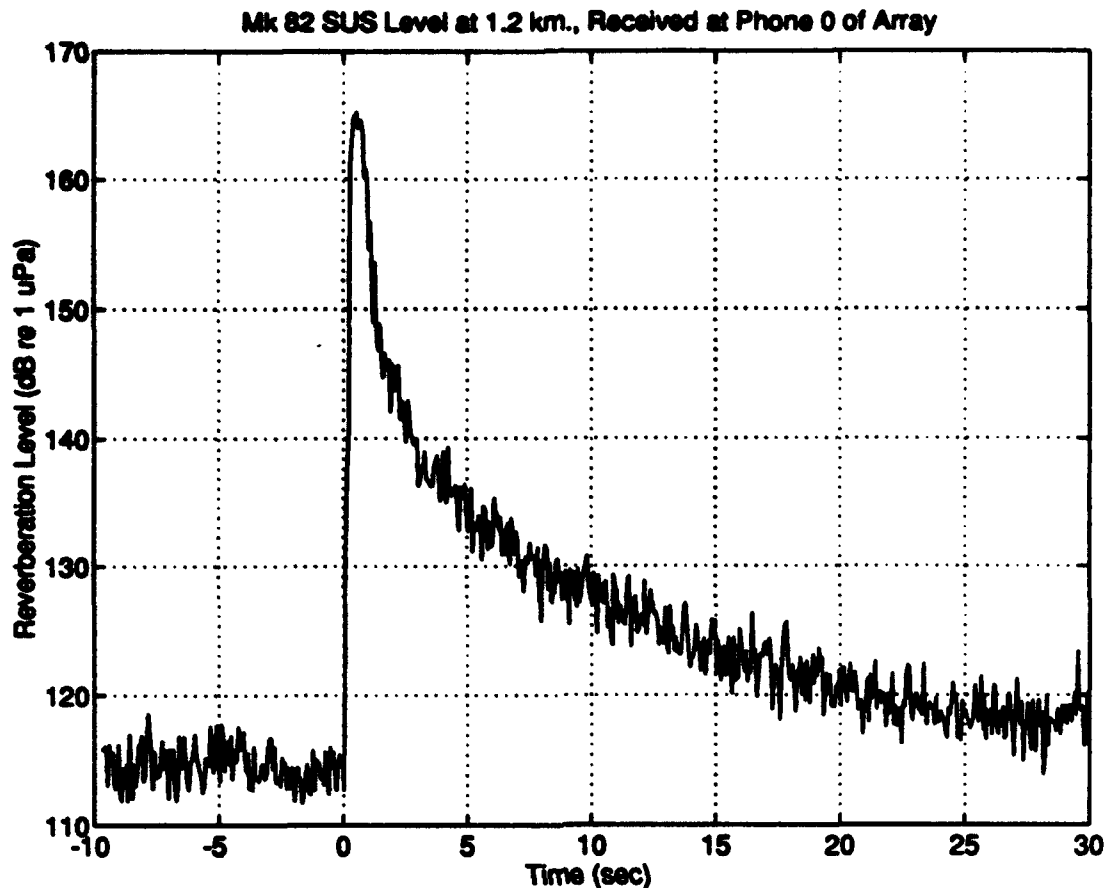
Figure 3.6: Reverberation following a 1.8 lb explosive charge (Mk 82 SUS) detonating at 91.4 m in water 275 m deep, as observed with a hydrophone at a depth of 121 m. Filter band 50 to 500 Hz.

contribute to the reverberation. Only one of these multiple scattered angles is the monostatic return; the scattering is thus bistatic in elevation. As will be shown in Chapter IV, the scattering is in fact bistatic in azimuth also.

In Chapter IV, the method used to predict bottom reverberation in the Barents Sea will be based on an implementation of Lambert's law in shallow water taking advantage of the vertically bistatic nature of $S_{Lambert}$. This problem could not be attacked in this manner in the past because of the lack of adequate computing power.

37

3. Omnidirectional Scattering

The general form of the omnidirectional scattering theory, also known as the Lommel-Seeliger law, is (McCammon, 1993):

$$S_{omni} = 10 \log(\mu \sin\theta_0) = \mu_{dB} + 10 \log(\sin\theta_0) \qquad (3.15)$$

Again, μ_{dB} is dependent upon the bottom sediment properties, frequency, and azimuth (of the scattered energy). This theory differs from Lambert's law in that it only depends on the sine of the incident energy's grazing angle. McCammon (1993) argues that at low grazing angles (less than $30°$), both monostatic and bistatic data support the first power dependence on $\sin(\theta_0)$. This theory will be tested in Chapter IV.

C. UNDERWATER EXPLOSION THEORY

Underwater explosions have been used for many years as acoustic source in many diverse applications (Weston, 1960):

- Geophysical prospecting, especially by the oil industry (where their use has been quite successful).

- Underwater signaling, including distress signaling.

- Sound sources for explosive echo ranging against submarine targets (though such use is not popular among submariners, including the author).

- Underwater sound propagation experiments, including reverberation studies.

In the latter application, they have become the *de facto* standard source due to their energy density, near impulse-like characteristics, and low cost. They also have distinct advantages over other impulse-like sources (such as sparkers) in that they are easy to deploy and are not limited in depth. This is not to say they are perfect, however, since

the signal they produce is somewhat random and is riddled with distinguishing characteristics which vary depending on the type of explosive/detonator, the fusing mechanism, the size of the charge, and the depth of detonation. Since they have been used for so long, many of these characteristics have been measured and quantized, and hence they have become relatively predictable sources of sound.

1.   The Underwater Explosion and Gas Globe

When a high explosive is detonated, the detonation wave propagates through the mass of explosive material, converting it to an incandescent gas at a very high pressure. In high explosives like TNT, this detonation wave or "shock" wave is supersonic with velocity between 5,000 and 10,000 m/s. A spherically symmetric shock wave is then radiated into the surrounding water with a pressure rise that is practically instantaneous, followed by an exponential decay with a time constant on the order of a fraction of a millisecond. The gas bubble or "globe" created by the explosion grows with the shock wave, but due to inertia it overshoots its equilibrium radius, and hence the radiated pressure becomes slightly negative as the bubble begins to contract. As it contracts it again overshoots its equilibrium radius, and when it reaches its minimum volume, a positive pulse with strength and duration comparable to the initial shock wave is developed. Successive pulses grow increasingly weaker. This damped radial oscillation continues, creating positive pulses at each point of minimum radius, until the globe either reaches the surface or breaks up into smaller parts. The oscillatory signal of these explosions is known as the *bubble pulse*. The pressure signature of an underwater explosion at short ranges consists of the shock wave followed by a small

number (less than 10) of bubble pulses. At longer ranges or in shallow water, the received signal is complicated by multipath effects which create more positive and negative impulses for each path, with surface reflections causing negative-going impulses. (Weston, 1960, and Urick, 1983)

2. The Bubble Pulse

The time difference between the shock wave and the first bubble pulse is determined by the weight of the charge, the type of explosive, and the depth at which it is detonated. This time difference T is predictable and can be found theoretically (Urick, 1983):

$$T = \frac{Kw^{1/3}}{(d+33)^{5/6}} \tag{3.16}$$

K depends on the type of explosive ($K = 4.36$ for TNT), w is the charge weight in pounds, and d is the detonation depth in feet. The reciprocal of T is known as the *bubble pulse frequency* and is measurable from data. For a Mk 82 SUS charge detonating at 300 ft, the predicted bubble pulse frequency is 23 Hz, which agrees well with the Barents Sea data. This measurement is important, since it proves that the SUS charges were detonating at the correct depth with the correct strength in the shock wave.

Energy is radiated as long as the bubble continues to oscillate, but for large charges and shallow depths (i.e. when the bubble is large), the bubble rises appreciably during one oscillation, resulting in a new source depth and a different multipath problem. Additionally, it affects the energy spectrum of the source, since the frequency of oscillation will shift as the bubble migrates toward the surface. Because of the possible

40

implications of this *bubble migration*, it is important to know when the effect is significant. Weston (1960) proposes that the critical depth below which this effect is small is given by

$$d_0 \sim 200 W^{(1/4)} \qquad (3.17)$$

where W is the charge weight in pounds. This corresponds to 232 ft for a 1.8 lb charge. Since the Mk 82 SUS detonated at 300 ft, bubble migration is not a concern in the BSPFEX.

3. The Energy/Power Spectral Density

Since the pressure signature of a SUS is by its very nature random, it is necessary to move to the frequency domain in order to avoid complications caused by modeling such an explosion in the time domain. This shift also entails a choice of either *energy flux density* or *power spectral density* of the shock wave and first few bubble pulses (which contain almost all of the energy generated by the explosion). This thesis will use power spectral densities in units of decibels referenced to $1 \ \mu Pa^2/Hz$ @ 1 meter. Weston and Urick both provide spectra for charges. Weston's work, while excellent, is somewhat dated. Urick includes a disclaimer with his spectrum calculation in which describes his curves are, "based upon, and are useful only for, broad-band levels, and are misleading for narrow-band work in not showing the fine-frequency spectral variation caused by the multipulse character of an explosive signal." (Urick, 1971) Hence, a more recent source is needed.

41
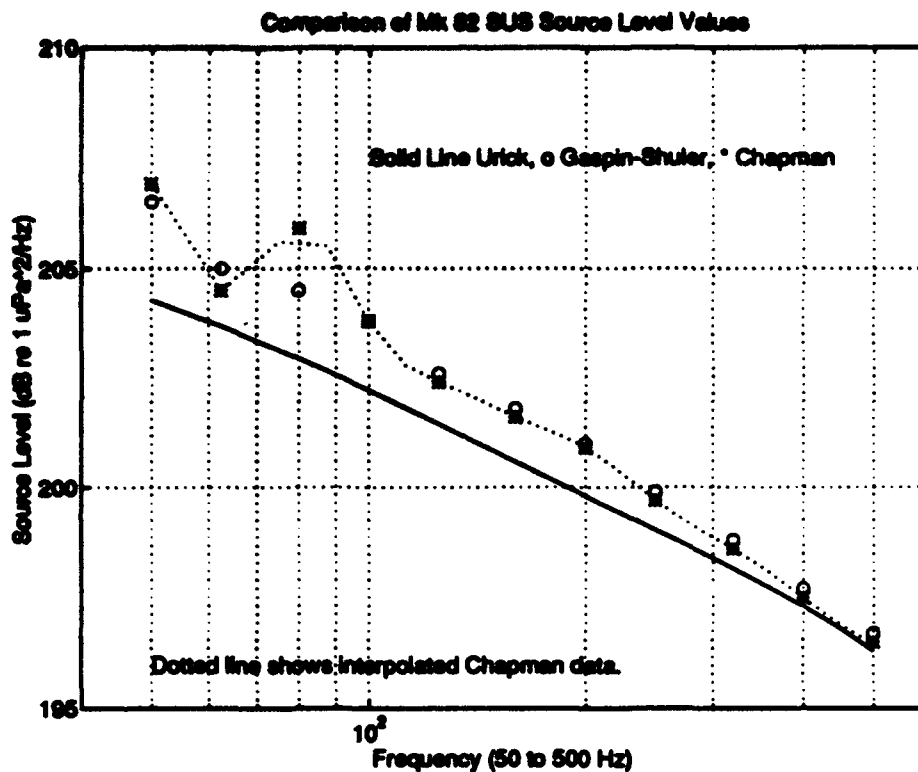
Figure 3.7: Comparison of Mk 82 SUS source level spectra.

Subsequent to the above researchers, source level measurements for various types of charges were made by Stockhausen (1964), Christian and Blaik (1965), Turner and Scrimger (1970), Gaspin and Shuler (1971), and Chapman (1987). Prior to Chapman, the most widely used values for the source levels of shallow SUS were Gaspin and Shuler's. Their estimates were derived from hand-drawn waveforms that were based on experimental measurements of the waveforms of deep explosions extrapolated to shallow depths. Between Gaspin and Shuler's work and Chapman's, there were several measurements performed that were in general agreement with the Gaspin and Shuler

predictions, but there were considerable differences among the data sets. (Chapman, 1987)

Chapman's results are presented in 1/3 octave bands from 5 to 630 Hz. At least 30 charges (1.8 lb SUS) were averaged for each detonation depth reported. The standard deviations were within 1 dB for most frequency bands (from 50 to 500 Hz all standard deviations were less than 1 dB). Chapman notes that actual explosion depths were consistently deep in all measurements. He theorized, with support from a previous experiment, that this was due to the relatively cold water (9° C) in which the experiment was conducted. Instead of the charges averaging the nominal 91.44 m (300 ft), he noted an average depth of 99.6 m (326 ft). This effect should be insignificant in the BSPFEX, as the effect on bubble pulse frequency is slight. Also, since the propagation model assumes a monostatic problem, a deeper detonation actually moves the detonation closer to the top of the array, making the monostatic assumption more viable.

Chapman's results agree well with Gaspin and Shuler's, with the possible exception of the lower frequencies. Chapman points out clearly, however, that this effect was expected because Gaspin and Shuler did not specifically account for the impulse of the waveform, which would throw off their low frequency predictions (Chapman, 1987). In this thesis, the source levels measured by Chapman will be used, utilizing interpolated values (cubic spline fit) to obtain an approximate source level every 12.5 Hz from 50 to 500 Hz. This is shown by the dashed line in Figure 3.7.

In the following chapter, the SUS model will be used as part of the input for a reverberation envelope prediction system designed for the Barents Sea. The predictions made by the system will then be compared to the shot data to validate its performance.

IV. METHOD AND RESULTS

A. PREDICTION METHOD

As described in Chapter I, propagation modeling for the Barents Sea has been performed using ray traces provided by HARPO. The propagation model from HARPO is then used along with the SUS source model described in Chapter III and either Lambert's law or omnidirectional scattering bottom backscattering functions to produce a predicted reverberation envelope. Each of the components in the prediction routine are described in the sections below.

1. HARPO

HARPO (Hamiltonian Acoustic Ray-tracing Program for the Ocean) is a FORTRAN computer program that traces the three-dimensional paths of acoustic rays through model oceans by numerically integrating Hamilton's equations, which are a differential expression of Fermat's principle. It was developed by R. Michael Jones, J. P. Riley, and T. M. Georges at the Wave Propagation Laboratory in Boulder, Colorado (an Environmental Research Laboratory of the National Oceanic and Atmospheric Administration). As described in Jones, et al. (1986), it uses continuous models for the sound-speed distribution and bathymetry in the ocean, hence avoiding the false caustics and discontinuous raypath properties encountered in conventional ray-tracing methods. Only geometrical effects are accounted for in the ray-trace; that is, no diffraction or

45

partial reflection corrections are applied by HARPO itself. Amplitude along a raypath is not explicitly computed; that is left to a post-processing program which accounts for boundary interactions and losses due to ray tube spreading and absorption. The program does produce a step-by-step account of each ray's progress, including all turning points and boundary interactions, and outputs the data in machine-readable form for post-processing. The post-processing tool chosen for this thesis was MATLAB.

The inputs for HARPO in its present form (on the Naval Postgraduate School's Cray Y-MP EL98) are a data file which contains the three-dimensional sound speed field in the region (sound speed at each longitude/latitude/depth point), a data file which contains the two-dimensional bathymetry for the same region (depth at each longitude/latitude pair), the source/receiver location, the desired launch elevation angles, and the desired launch azimuth. It then computes closed-form expressions for the bathymetry and the sound speed field using a user-specified number of "empirical orthogonal functions" (EOF's) to model the sound speed field (Chiu, et al., 1993). The number of EOF's required depends on the original number of sound velocity profiles (SVP's) entered and the maximum error desired in the continuous representation of the field.

It should be noted that HARPO cannot directly compute the raypaths that connect a specified source and receiver (or scatterer in the case of reverberation). To find such *eigenrays*, one usually launches a fan of rays at small increments in elevation and/or azimuth angle and linearly interpolates for the rays that reach the desired receiver location. In the specific case of bottom reverberation, since each bottom interaction is
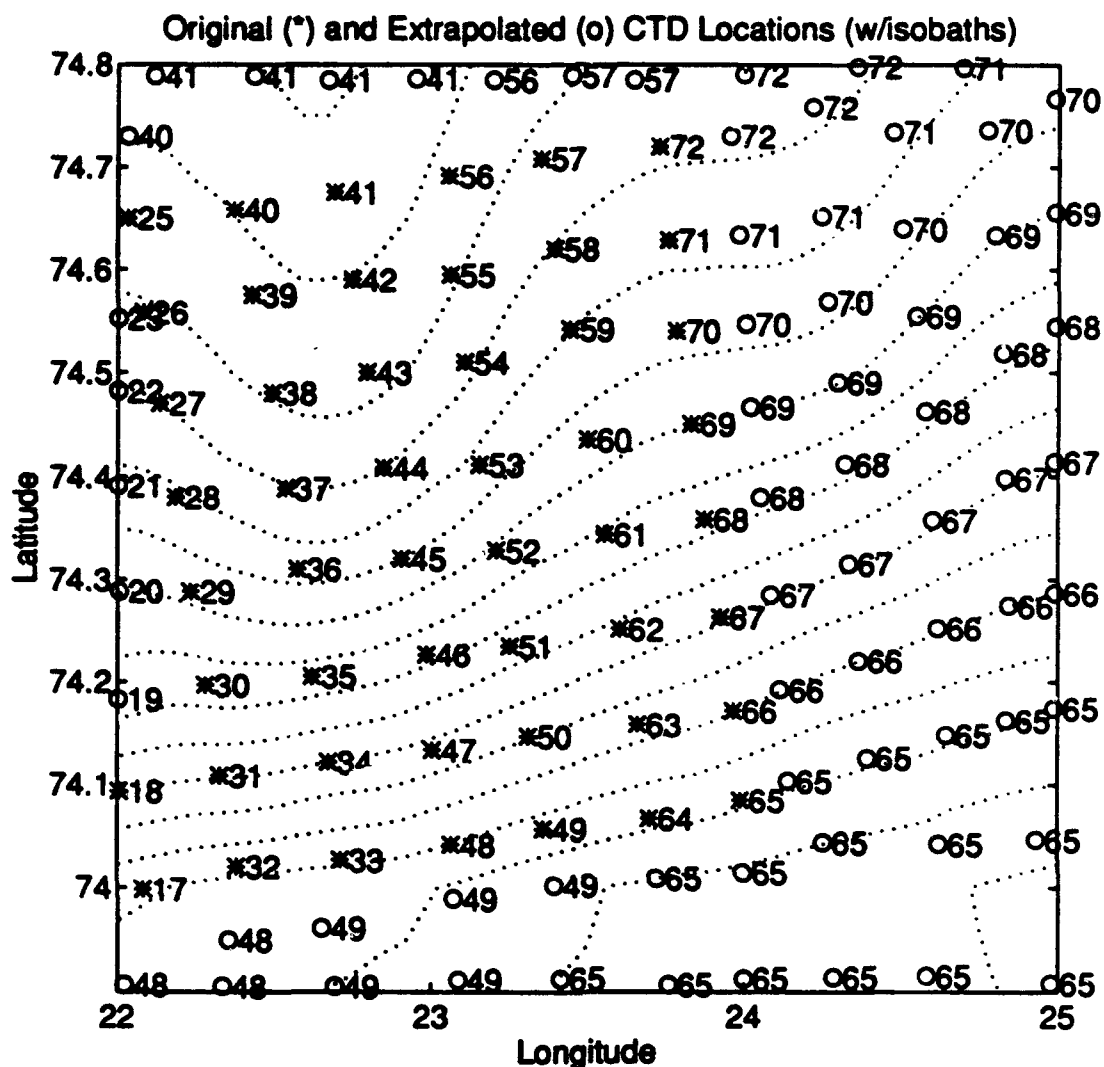
Figure 4.1: CTD locations and extrapolated points along isbaths.

identified in HARPO's output "rayset," this turns out to be an interpolation along the bottom only (assuming the bottom is locally flat).

The bathymetry for the Barents Sea was obtained using the WORLDBATHY database in the Naval Postgraduate School's Oceanography laboratory. The data originally came from DBDB5, a standard U. S. Navy world bathymetric database. The sound speed field was measured as part of the BSPFEX. A total of 72

Conductivity/Temperature/Depth (CTD) measurements were taken, 56 of which were within 38 km of the array and hence were usable in the reverberation experiment. To cover the entire area, the CTD measurements were copied to new locations along isobaths, smoothed using an 11 point Hamming smoother, and then an inverse distance algorithm (*MATLAB*, 1992) was applied to interpolate the sound velocity field at regular grid locations for 10 longitudes and 9 latitudes around the array. For the three-dimensional sound speed field in the Barents Sea experiment area, a total of 90 SVP's were used to estimate the sound speed field. To keep error less than 0.1 m/s, 26 EOF's were required.

To estimate the horizontally bistatic nature of the experiment (the source SUS and receiving array were ~1 km apart) using a monostatic propagation model, a source/receiver position that was in the center of the SUS drop points and array location was used. From that point, rays were launched on several azimuths over a fan of elevation angles. The runs were originally performed using a three-dimensional environment, but it was quickly discovered that doing so violated the assumptions made in modeling the reverberation using an N x 2D approximation. To correct this discrepancy, the final HARPO runs were performed using two-dimensional "slices" from the three-dimensional environmental data. Four launch azimuths (000, 090, 180 and 270) were used, with rays traced every 0.5° in elevation from -60° to -20° and from +20° to +60°, and every 0.1° in elevation from -20° to +20°. The results of both the 2D and 3D data runs are described later in this chapter.

48

2. Post-processing of HARPO: rbreakbr.m

rbreakbr.m is a MATLAB script which reads in the output data file from HARPO and processes it to find eigenrays between the source/receiver location and desired range points along the azimuth on which HARPO was run. For each eigenray to a given bottom point, it determines the ray's amplitude, path length, horizontal range, depth, phase, arrival angle and travel time. The local sound speed at the bottom, original launch angle of the ray, and vertical distance between it and the adjacent ray used for ray tube spreading calculation are also stored.

Ray path lengths are determined by simply summing the straight line distances between HARPO rayset output points. Stepping through all output points for each ray, boundary interactions and turning points are accounted for individually. At each, the type of interaction is identified and numbered using a system described by Franchi et al. (1984). Each interaction or turning point is numbered as an *order contour*, with all surface interactions/upper turning points receiving odd numbers, and bottom interactions/lower turning points even. If the first interaction is a bottom interaction, it is hence identified as #2. Each is also identified as to the type of point (boundary interaction or turning point). This numbering method turns out to be key in later processing when interpolation is performed between adjacent launch angle rays at bottom interactions with the same order contour.

Amplitude calculations for a ray at a given bottom interaction are determined by the combined effects of surface and bottom interactions the ray has experienced up to that point and ray tube spreading. At each surface interaction, the loss mechanism

49

assumed is due to scattering loss only using the Eckart coherent reflection coefficient R_c such that

$$R_c = \Re e^{-2\gamma^2 \sigma_{bottom}^2} \qquad (4.1)$$

where $\Re$, the Rayleigh reflection coefficient, is equal to 1, $\sigma_{surface}$ is the rms waveheight in meters (less than 0.1 meter during the experiement; 0 meters used in analyses), and γ is the horizontal wave number (Tolstoy, et al., 1987). For each bottom interaction, the loss mechanism assumed is due to scattering loss using the Eckart coherent reflection coefficient along with $\Re$. For angles less than critical (68° for the bottom in the vicinity of the array, as measured using the ground wave of the SUS charges) the magnitude of the Rayleigh reflection coefficient is 1. Rays which have angles higher than this are so severely attenuated that their contribution to the reverberation level is insignificant. Hence, the magnitude of the specularly reflected ray after a bottom reflection is also determined by Equation 4.1, where σ_{bottom} is the rms roughness of the bottom in meters (Tolstoy, et al., 1987). σ_{bottom} was determined from fathometer recordings to be approximately 0.5 meters. At the frequencies of interest in the BSPFEX, loss due to absorption in the bottom is negligible. Ray tube spreading is calculated using conservation of power within the ray tube given by the following equation:

$$\frac{P}{P_0} = \sqrt{\frac{\Delta\theta_0}{rh}\frac{\rho c}{\rho_0 c_0}\left|\frac{\cos(\theta_0)}{\cos(\theta)}\right|}$$ (4.2)

P is the acoustic pressure at horizontal range r from the source, P_0 is the acoustic pressure 1 meter from the source, $\Delta\theta_0$ is the angular difference, in radians, between adjacent launch angle rays, h is the vertical distance between the two rays at range r, ρ and ρ_0 are the water densities at the bottom point and at the source (assumed equal), c and c_0 are the sound speeds at the bottom point and at the source, θ_0 is the launch elevation and θ is the elevation angle of the ray at the bottom interaction (Clay, et al., 1977).
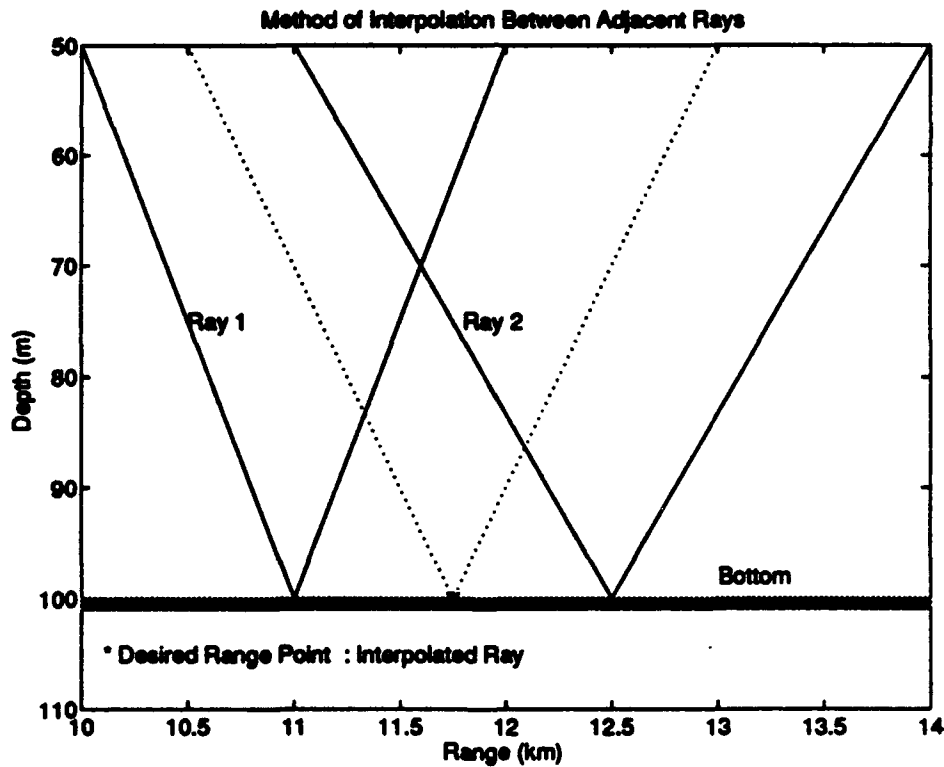

Figure 4.2: Notional view of interpolation between adjacent launch angle rays.

Once all bottom interactions have been identified and eigenray data for each has been stored, the program then steps out in range to the points specified (at regular intervals) and finds adjacent launch angle rays which have bottom interactions with the same order contour which "straddle" the desired bottom point. This is illustrated graphically in Figure 4.2, where the two solid lines represent adjacent launch angle rays (which have bottom interactions with the same order contour) which straddle the location of a desired output point on the bottom. A linear interpolation is then performed in range, assuming the bottom to be locally flat, to find ray amplitude, path length, depth, phase, travel time, arrival angle and local sound speed at the desired point.

3. Combining Eigenrays, SUS Model and Scattering Function: rlmaker.m

The goal of the *rlmaker.m* routine is to estimate the reverberation level prediction algorithm suggested by Franchi, et al. (1984) and more recently by Bucker, et al. (1993). They both suggest a double integral over the reverberating area with multiple eigenrays connecting each "patch" *dA* on the bottom with the source/receiver. In order to model reverberation in this manner using a true three-dimensional model, ray traces would have to be done from each SUS location over a fan of launch elevations for each azimuth in a 360° fan surrounding the SUS. A similar run would have to be done for each of the other three SUS and for the vertical line array. Then, rays connecting the SUS and the vertical line array with a given patch on the bottom would have to be picked out of the set, and the appropriate amplitude/travel times assigned to each. This is a formidable task, yet Bucker, et al., claim to have successfully modeled reverberation in this way with some simplifications in their RUMBLE product (Bucker, et al., 1993).

52

Confining the problem to a two-dimensional slice of the ocean and assuming a horizontally monostatic problem lessens the computational load significantly, and enables the routine to run within a reasonable amount of time. It also ensures that the rays connecting the source to a given scattering patch are the same as the rays which connect that patch back to the receiver. The reverberation level at the receiver due to a source with intensity $I(t)$ is thus

$$R(t) = \iint_A \sum_{i \in m(r)} \sum_{j \in m(r)} I(t - T_i(r) - T_j(r)) \frac{B(\theta_{i0}, \phi_{i0}) \bar{B}(\theta_j, \phi_j)}{L_i(r) L_j(r)} \sigma(\theta_i', \theta_j') \, dA$$

(4.3)

The two T terms represent the travel times along the ith raypath from the source to the bottom point and for the jth return path in the set of raypaths represented by the set $m(r)$ connecting the source/receiver and the bottom patch dA which is at range r. The two B terms represent the beamforming factors to be taken into account on the source and receivers and the two L terms account for losses in amplitude. σ is the scattering strength of the bottom, depending on the incident energy grazing angle θ_i' and the scattered energy's launch angle θ_j'. No azimuthal dependence is modeled. This method is displayed graphically in Figure 4.3.

Franchi et al. note that it was not possible for them to evaluate Eq. 4.3 directly due to a lack of a three-dimensional propagation model. Bucker et al. were able to evaluate the intergral because they had both the model and the required computing assets. At the Naval Postgraduate School, there were adequate computing facilities and a three-dimensional propagation model, but the run time required to properly model the
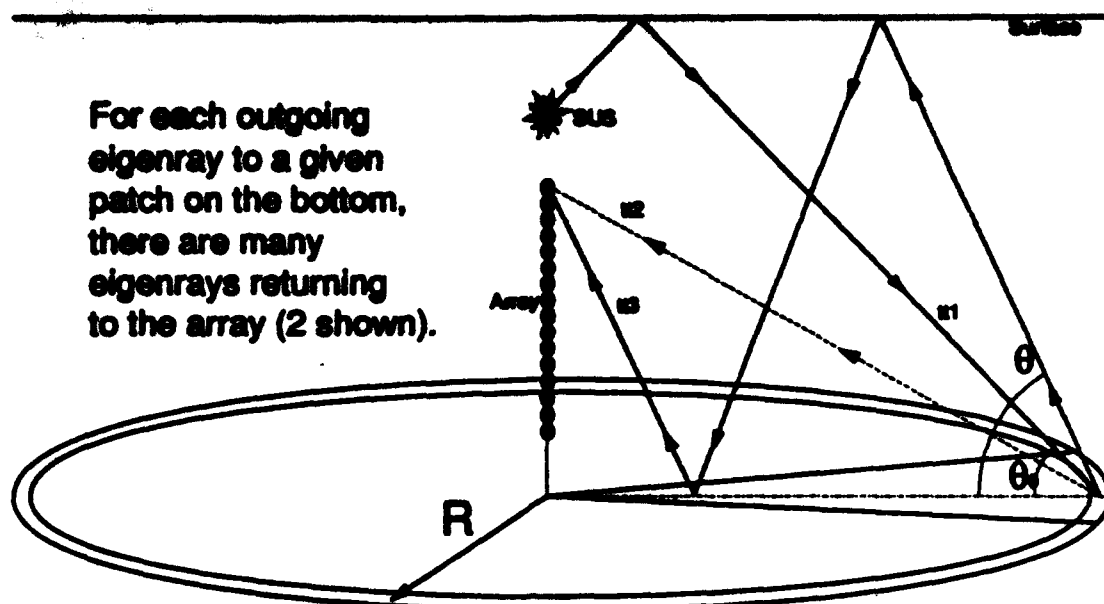
53

Figure 4.3: Illustration of multipath reverberation problem.

reverberation in shallow water proved prohibitive at the time of this writing.

Given the asssumptions stated above, and estimating the area integral by summing the contributions to reverberation by rings on the bottom, Eq. 4.3 simplifies to

$$RL(t,f) = \sum_k \sum_i \sum_j B\ I(t-T_i-T_j,f)\ \frac{1}{L_i(f)L_j(f)}\sigma(\theta_i,\theta_j,f)\ \pi(r_{k2}^2-r_{k1}^2) \quad (4.4)$$

B is now the effective beamwidth of the point source/receiver given the region for which the ray trace is applicable. For the four azimuth approximation to be made, $B = 0.25$. $I(t,f)$ is the intensity of the SUS at frequency f and is assumed constant at its peak level for 0.1 sec. The summation over k performs a power sum of the contributions from each ring out to a range of ~38km, placing the reverberant energy into the appropriate 0.1 second time bin depending on the two-way, vertically bistatic travel time of the ij raypath. The two loss terms and the bottom backscattering strength are frequency dependent. r_{kl}

54

and r_{k2} represent the inner and outer radii of the kth ring which has its center at $(r_{k2}+r_{k1})/2$, and such that rings do not overlap. Hence, $RL(t,f)$ is the predicted reverberation peak envelope at the desired frequency.

B. BARENTS SEA DATA ANALYSIS

To most closely estimate a monostatic problem, only the phone closest to the detonation depth, phone 0, the top phone, was analyzed for reverberation level. Broadband peak level measurements were performed using a peak picking algorithm and a straight conversion from voltage to sound pressure level in decibels:

$$RL(t) = 20 \log(voltage \times 10^8) \qquad (4.5)$$

Voltage levels were corrected for phone sensitivity problems and non-zero mean as described in Chapter II.

Narrowband measurements were performed using a Short-Time Fourier Transform (STFT) power spectral density estimate using an $N = 128$ point rectangular window, with 1/2 window overlap in segment intervals (Therrien, 1992). If the fast Fourier transform (fft) of data vector $x(t)$ is given by $X(f)$, then the narrowband level of $x(t)$ in a 1 Hz bandwidth is given by

$$RL(f) = 20 \log\left(\frac{2 X(f) X^*(f)}{N f_s}\right) \qquad (4.6)$$

f_s is the sampling frequency (1600 Hz). The factor of 2 is required to maintain conservation of power when only considering positive frequency. Prediction results and

C. PREDICTION RESULTS

Narrowband predictions were made for 1 Hz bandwidths centered at 50, 100, 200 and 400 Hz. In the process of developing the results, the backscattering coefficient of the Barents Sea has been determined. Both Lambert's law and omnidirectional scattering were considered. In general, the choice of the backscattering function tends to change the slope of the estimate with time, while the choice of the backscattering strength shifts the estimate up and down without slope change. Lambert's law provides a better fit to the measured data. The values of μ in Table 4.1 were found to best fit the Barents Sea data. They are consistent with the findings of McCammon (McCammon, 1993).

TABLE 4.1: BACKSCATTERING STRENGTH PARAMETER μ FOR SEVERAL FREQUENCIES IN THE BARENTS SEA.

Frequency (Hz)	50	100	200	400
μ (dB re m^2)	-40±15	-37±10	-28±7	-20±7

Determination of which scattering function is better is somewhat subjective, in that the choice of parameters in the propagation model determine which scattering function fits better. Figure 4.4 demonstrates this by showing the difference obtained using Lambert's law and omnidirectional scattering. Any loss term which increases with range also changes the slope of the estimate, more dramatically, in fact, than the choice of the

56

scattering function. Specifically, volume absorption, surface scattering loss, bottom scattering loss, and bottom absorption are all loss terms which tend to act in a roughly linear manner to increase transmission loss (TL in decibels) with range. Therefore, perfect, or near perfect, propagation modeling is required in order to determine which scattering function is more accurate. In shallow water, this may not be a reasonable request, especially given the nature of the multipath problem.
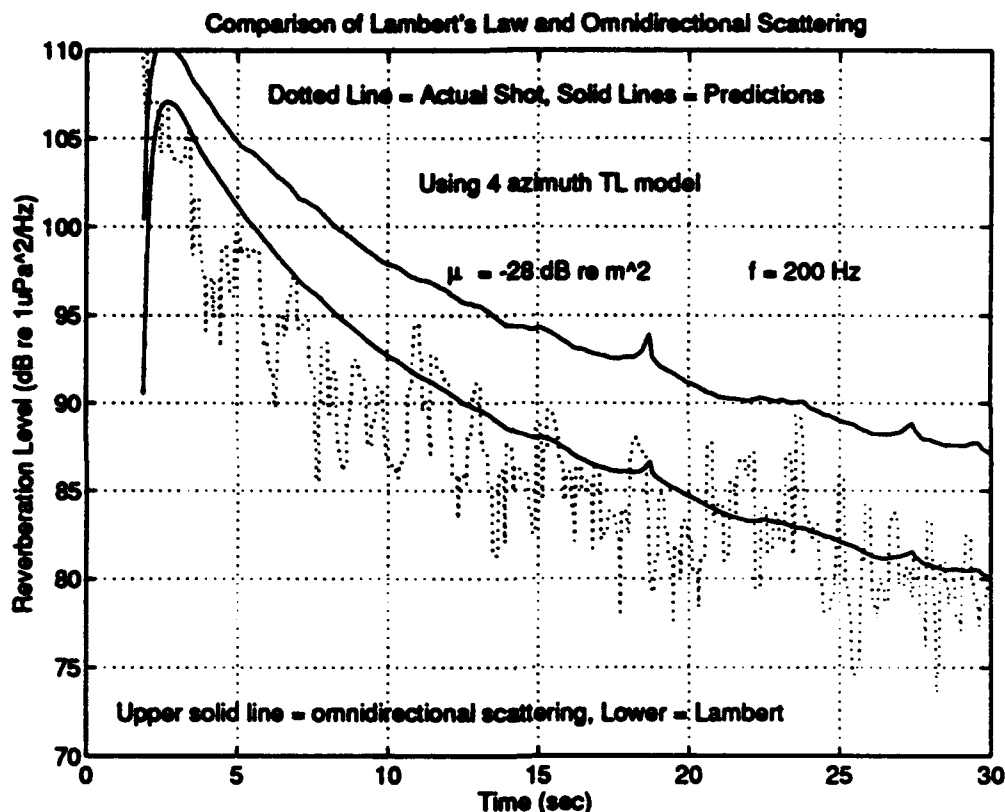

Figure 4.4: Comparison of Lambert's law with omnidirectional scattering at 200 Hz, overlaid on 200 Hz data from the BSPFEX.

Figures 4.5 through 4.8 show the predictions and data collected during the BSPFEX that generated the numbers in Table 1. At 50 and 100 Hz, the propagation model is suspect for two reasons. The first is the lack of an adequate loss mechanism to fully

explain the slope of the BSPFEX data. This is especially visible at 50 Hz, as the prediction begins to increase at the 20 second mark. The second reason is the more fundamental question of whether ray theory is correct at lower frequencies. For these reasons, the predictions at 200 and 400 Hz are thought to be much more accurate than those at the lower frequencies. For the validity of these models to truly be determined in a general sense, a closer examination is required using data from several different regions.

The trend indicated in the rising μ with frequency is significant. It is also consistent with rough surface scattering theory as described in Chapter III. Referring back to Equation 3.5, it is clear that the scattering function varies with f in a complicated fashion. From the predictions in Figures 4.5 through 4.8 and the values listed in Table 4.1, there appears to be between 3 and 8 decibels per octave difference in scattering strength over the frequency band considered. Again, this conclusion should be tempered with the knowledge that the propagation modeling may not be exact below 200 Hz.
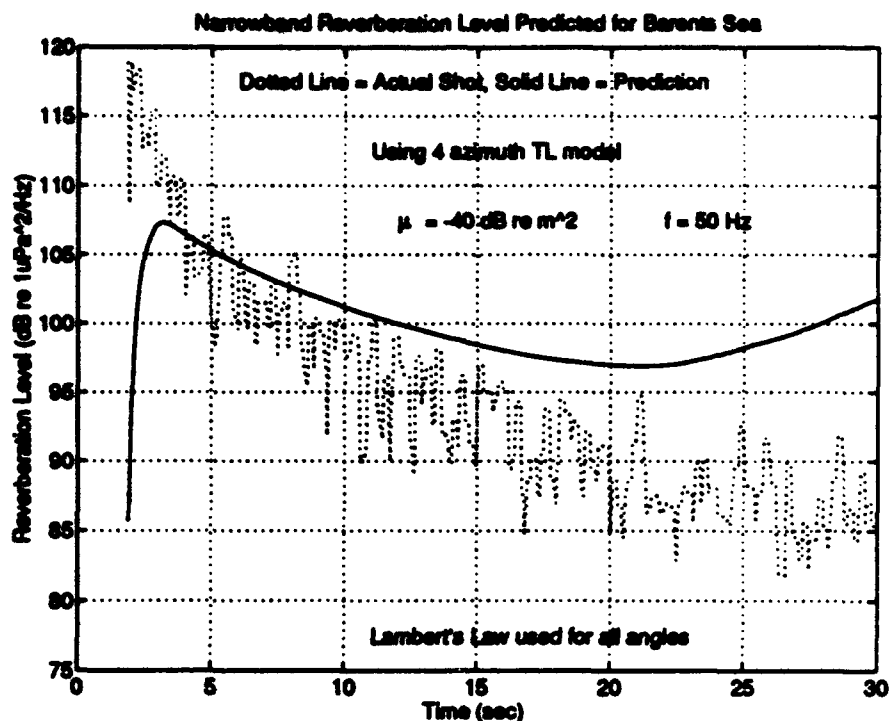
Figure 4.5: Reverberation level prediction and Barents Sea results at 50 Hz.
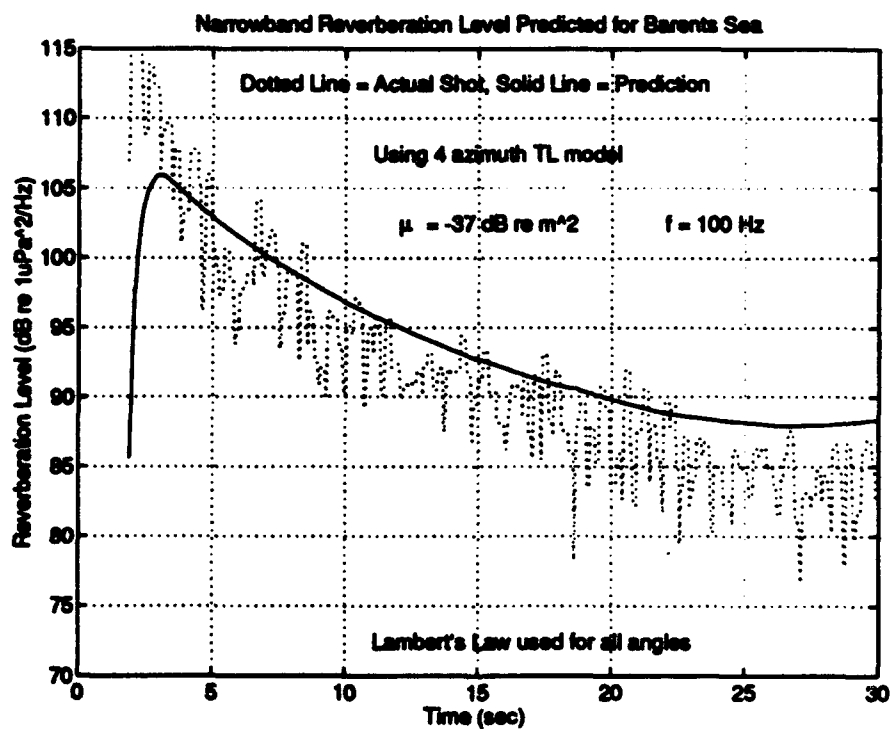

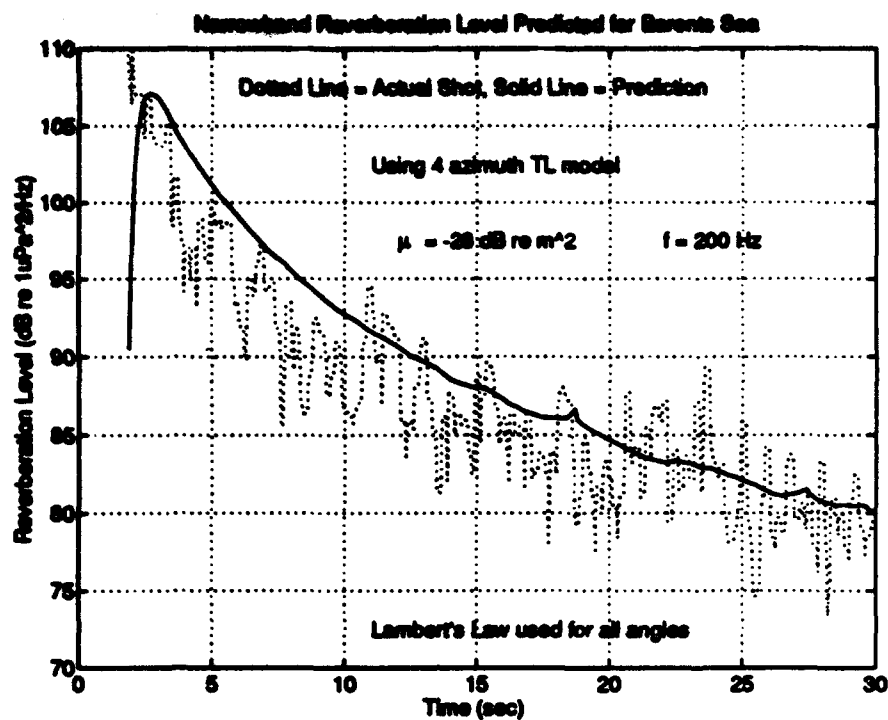**Figure 4.6:** Reverberation level prediction and Barents Sea results at 100 Hz.

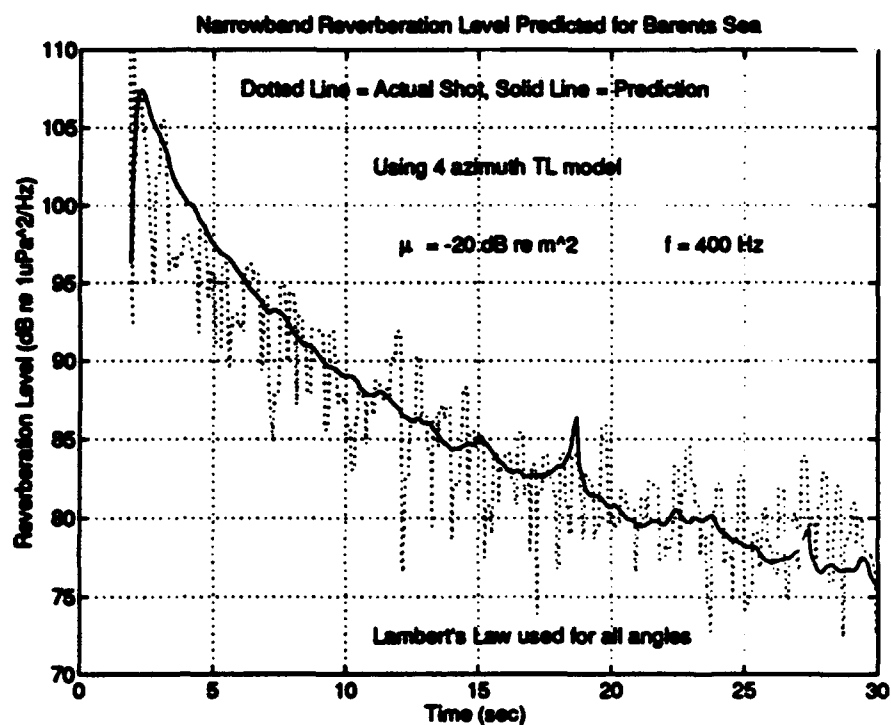**Figure 4.7:** Reverberation level prediction and Barents Sea results at 200 Hz.

Figure 4.8: Reverberation level prediction and Barents Sea results at 400 Hz.
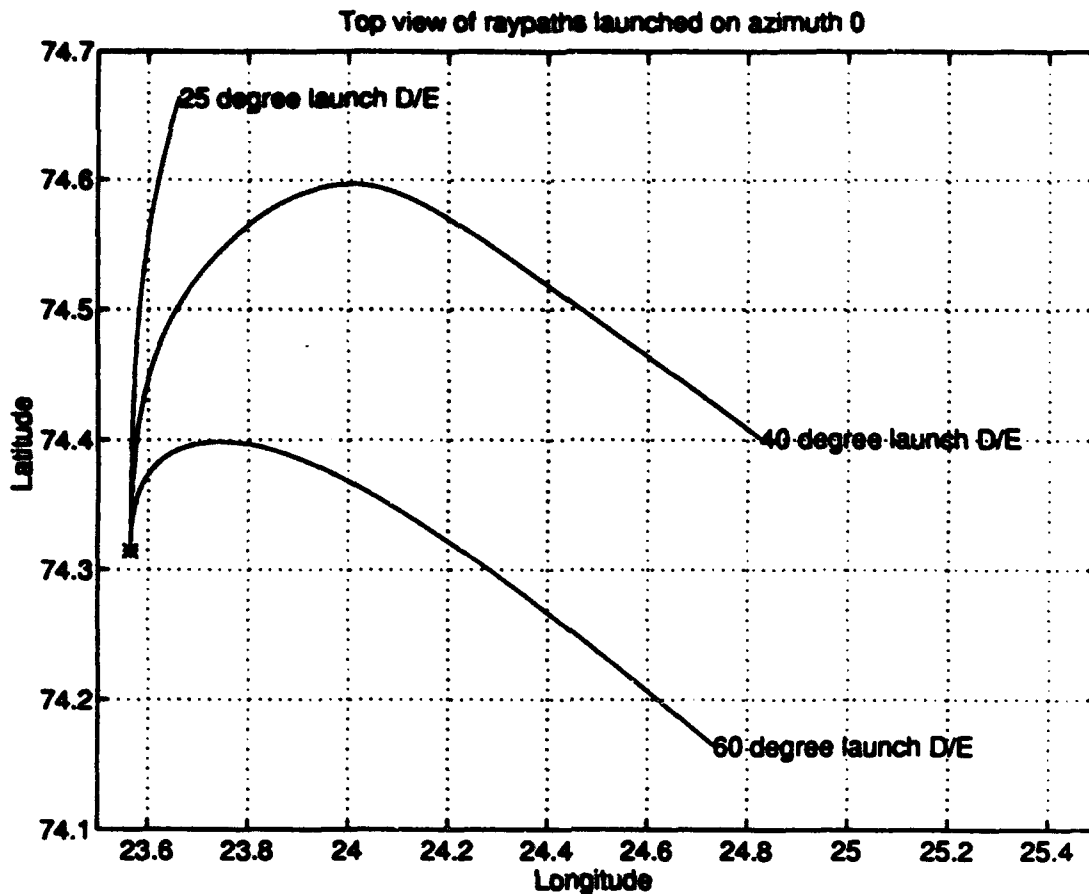
Figure 4.9: Plot showing horizontal refraction of three rays launched from the vertical array on azimuth 000T.

A significant effect not taken into account in the two-dimensional prediction routines is that of horizontal refraction. The significance of this effect is clearly illustrated in Figure 4.9. In it are shown the raypaths for three different launch angle rays (+25°, +40°, and +60°). The bathymetry proves to be the dominant effect on the rays as they refract eastward away from the shallow region to the northwest of the array. This causes a two-fold problem in the reverberation model. First, the assumption that a ray can be scattered to a return path with some angle other than its incident angle is invalid, unless a fan of launch azimuths is used along with a three-dimensional propagation

model. For example, assuming that a single launch azimuth will suffice for, say, a 90°
sector is incorrect, since this would imply that energy from a 25° launch elevation striking
the bottom at (74.65° N, 023.66° E) would somehow be scattered into a 45° received
elevation eigenray which emanated from (74.60° N, 024.00° E). This is simply not a
good assumption. Of course, modeling propagation in a three-dimensional environment
with a two-dimensional model is not a good assumption either, but at least doing so is
consistent with the method of reverberation prediction. The second problem is the effect
of horizontal refraction on signal amplitude due to ray tube spreading in the horizontal.
From Figure 4.9, this problem clearly appears to be significant. Hence, to accurately
model the reverberation in a shallow region, a three-dimensional model should be used.

D. STATISTICAL ANALYSIS

A statistical analysis of the BSPFEX data has been performed. Since the
reverberant return from an explosion in shallow water is by its very nature a non-
stationary process in time, the wideband returns (sampled at 1600 Hz) were broken into
5000 point segments and analyzed individually, assuming approximate stationarity over
the segment. The standard deviation σ_s of each segment was determined using
MATLAB, and the data segment was then divided by σ_s to normalize the segment to
standard deviations of pressure, a unitless quantity. This allowed segments to be
compared directly to determine the underlying probability density function of the entire
reverberation signal. Dividing the pressure by the standard deviation is essentially the
same as dividing by the rms pressure, or normalizing the signal power to one unit of
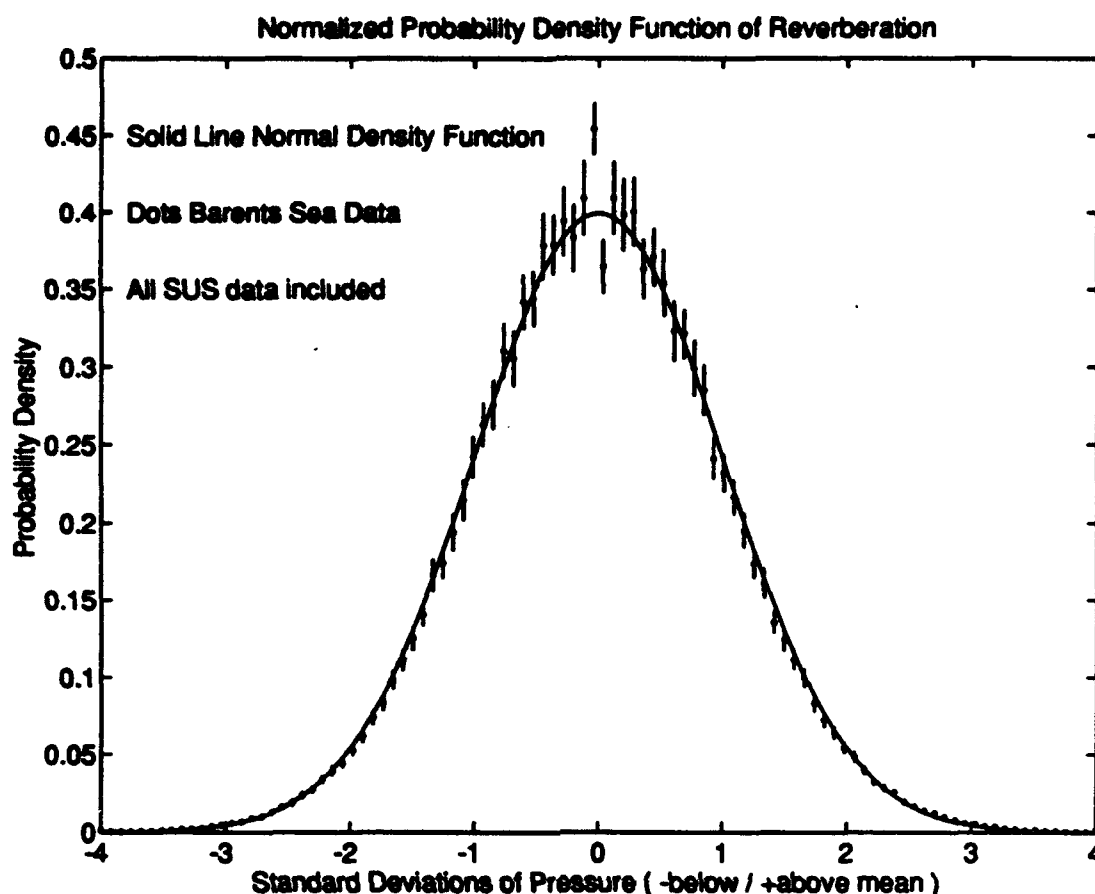
Figure 4.10: Normalized probability density function of reverberation signal. Dots show mean experimental values; vertical lines show 95% confidence intervals. Gaussian density overlaid for reference.

power. The probability density function $f_x(x^0)$ of each segment was then estimated using

the histogram subroutine in MATLAB (1992) and the equation:

$$f_x(x^0) \approx \frac{K_{x^0}}{K \Delta x} \qquad (4.7)$$

where K is the number of data points used for the estimate, Δx is the size of the analysis

bin in the histogram, and K_{x^0} is the number of data points which fell in the bin centered

on x^0 (Therrien, 1992). The average over time was also complemented with an ensemble

average over the four SUS returns to yield the mean probability density function shown in Figure 4.10. The dots on the plot represent the mean probability density function estimate over all four SUS returns, and the vertical line through each dot shows the 95% confidence interval determined using

$$\left[\bar{x} - \frac{\sigma'_x t_{n;\alpha/2}}{\sqrt{N}} \leq \mu_x < \bar{x} + \frac{\sigma'_x t_{n;\alpha/2}}{\sqrt{N}} \right] \tag{4.8}$$

where $\bar{x}$ is the sample mean of the random variable x, σ'_x is the sample standard deviation of x, $t_{n;\alpha/2}$ is the value of the Student t distribution for $n = N - 1$ (N is the number of data points in the sample x), and $\alpha = 1 - P$ for a ($P*100$) percent confidence interval. (Bendat, et al., 1971)

Clearly, the normalized wideband SUS returns have a stationary Gaussian distribution (i.e. a normal density function). Individual unnormalized segments are still Gaussian processes, but are not stationary since they have variance proportional to the instantaneous power of the return signal. The erratic estimate in the vicinity of zero standard deviations is due to quantization noise of the A/D converter in the measurement system. This noise becomes significant in the normalized data late in a given SUS return when the data is just barely above background noise.

In order to examine the statistics of narrowband data, the data were again segmented in order to compute fast Fourier transforms (fft's) of each 128 point segment. In order to prove that each frequency bin has a bivariate Gaussian distribution, the real and imaginary portions must be shown to both have Gaussian distributions. This was done
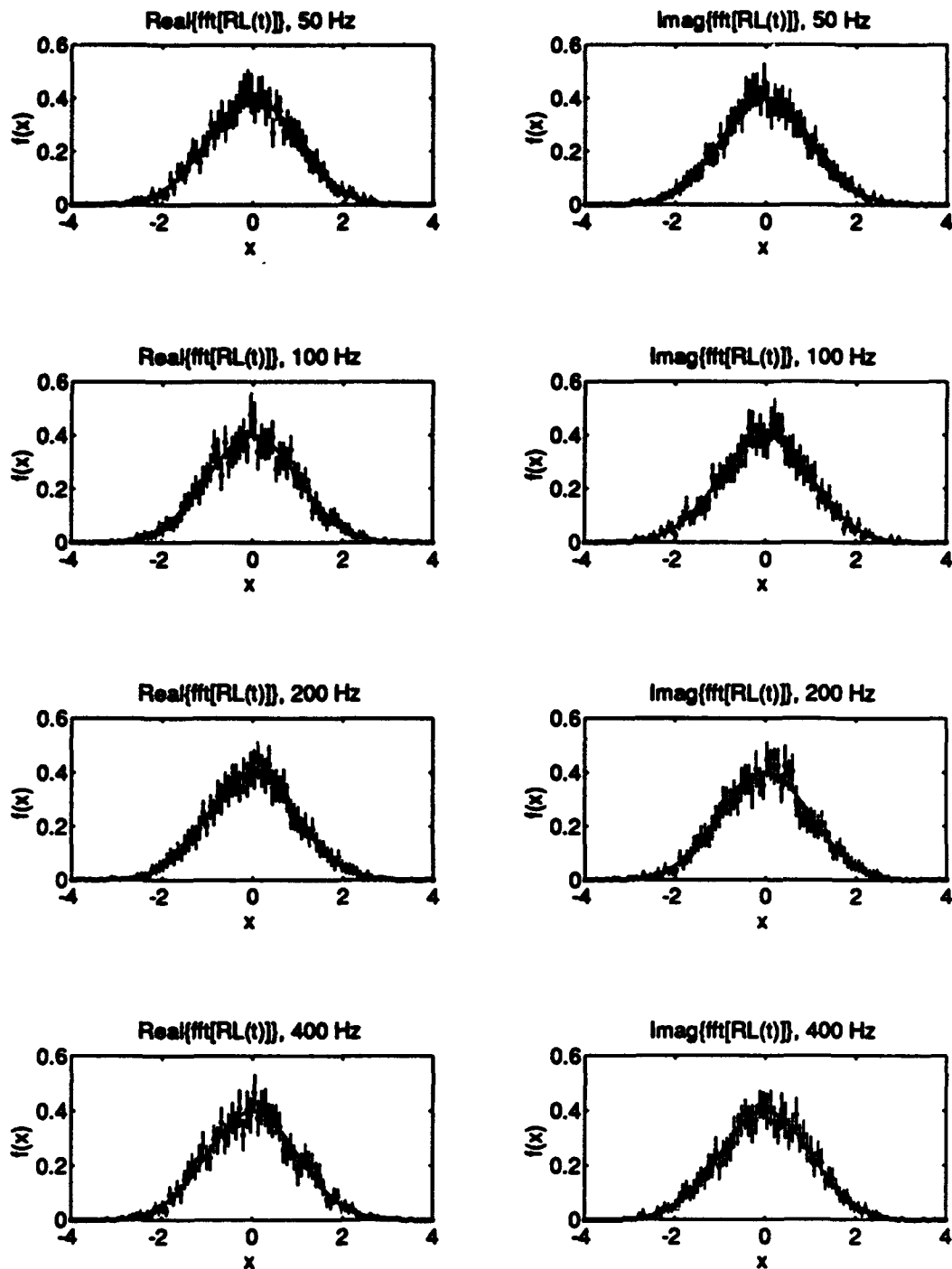
64

Figure 4.11: Narrowband probability density function estimates at 50, 100, 200, and 400 Hz. Dots show mean experimental values; vertical lines are 95% confidence intervals. Gaussian density function overlaid for reference.

using a method similar to that done on the wideband data described above. The results of this analysis are shown in Figure 4.11. As before, the dots represent the sample mean of the probability density function estimate over all four SUS charge returns. The vertical lines are the 95% confidence intervals. The narrowband data again clearly has a Gaussian distribution at all frequencies.

These results are significant, because verifying the signals to be Gaussian random processes allows a great deal of existing performance prediction algorithms to be applied in the analysis of active sonar systems in the Barents Sea. The results are not surprising, since the data comes from a multipath acoustic problem which is by nature random due to the effects of the oceanographic and bathymetric features over the entire azimuth. Nonetheless, they are quite valuable to a potential researcher or active sonar system model for the Barents Sea. This, however, does not necessarily imply that these results are true in general. In order to extend this assumption to other shallow regions, a similar study must be done for that region.

V. CONCLUSIONS

The objectives of this thesis were to consider several methods of reverberation prediction and compare these methods to the results from the BSPFEX, to determine the reverberant characteristics of the Barents Sea, and determine the statistical characteristics of the reverberation measured in the BSPFEX. The reverberation prediction routines which were developed for this shallow environment utilized multipath propagation modeling along with a vertically bistatic scattering function for the bottom. They have been used to accurately model the reverberation due to SUS charges dropped during the BSPFEX. It has been determined that Lambert's cosine law accurately describes the bottom backscattering function using a parameter which varies depending on bottom composition and roughness. Furthermore, that parameter has been determined at several frequencies for the Barents Sea. Omnidirectional scattering theory, however, has not been ruled out as a viable reverberation prediction tool. Finally, the statistics underlying the reverberant returns in the shallow water of the Barents Sea have been proven to be Gaussian distributions, both for broadband and narrowband data.

These results do not, by themselves, provide all the information required to predict the performance of a LFAA system in shallow water. They do however, provide key information which is necessary to achieve this goal. Knowledge of which scattering function to use and the parameters which drive the scattering is essential to predict

67

whether reverberation is a limiting factor. If it is, knowledge of the statistical properties of the reverberant returns is essential in such assessments.

Further research effort should be directed at modeling the reverberation in different shallow regions using different types of sources and receivers. Such modeling should consider three-dimensional effects both on propagation and scattering.

LIST OF REFERENCES

Barents Sea Polar Front Group (R. Bourke, C. -S. Chiu, J. Lynch, J. Miller, R. Muench, and A. Plueddemann), "Preliminary Cruise Results: Barents Sea Polar Front Experiment," unpublished, August 1992.

Bendat, Julius S., and Allan G. Piersol, *Random Data: Analysis and Measurement Procedures*, John Wiley & Sons, Inc., New York, 1971.

Bucker, Homer P., Joseph A. Rice and Newell O. Booth, "A Reverberant-Undersea Model for Bottom-Limited Environments," in *Ocean Reverberation*, ed. Dale D. Ellis, John R. Preston, and Heinz G. Urban, Kluwer Academic Publishers, Boston, 1993.

Chapman, N. R., "Source levels of shallow explosive charges," *Journal of the Acoustical Society of America*, 84 (1988), 697-702.

Chiu, C. -S., A. J. Semtner, C. M. Ort, J. H. Miller, and L. L. Ehret, "A ray variability analysis of sound transmission from Heard Island to California," accepted by the *Journal of the Acoustical Society of America: The Heard Island Experiment Special Issue*, 1993.

Clay, C. S. and H. Medwin, *Acoustical Oceanography*, John Wiley & Sons, New York, 1977.

Dyer, I., A. B. Baggeroer, H. Schmidt, J. R. Fricke, N. Ozluer, and D. Giannoni, "Discrete backscatter can be dominant in rough bottom reverberation," in *Ocean Reverberation*, ed. Dale D. Ellis, John R. Preston, and Heinz G. Urban, Kluwer Academic Publishers, Boston, 1993.

Emblidge, J. M., *A Feasibility Study of Ocean Acoustic Tomography in the Barents Sea*, Naval Postgraduate School Thesis, 1991.

Houstoun, R. A., *A Treatise on Light*, Longmans, Green and Co., New York, 1938.

Jones, R. M., J. P. Riley, and T. M. Georges, *HARPO: A Versatile Three-Dimensional Hamiltonian Ray-Tracing Program for Acoustic Waves in an Ocean with Irregular Bottom*, Wave Propagation Laboratory, NOAA, Boulder, Colorado, 1986.

Mackenzie, K. V., "Bottom Reverberation for 530- and 1030-cps Sound in Deep Water," *Journal of the Acoustical Society of America*, 33 (1961), 1498-1504.

MATLAB® Reference Guide, The Mathworks Inc., Natick, Massachusetts, August 1992.

McCammon, Diana F., "Low grazing angle bottom scattering strength: Survey of unclassified measurements and models and recommendations for LFA use," *U. S. Navy Journal of Underwater Acoustics*, 43 (1993), 33-47.

McLaughlin, P. G., *Signal-Processing for the 1992 Barents Sea Tomography Experiment*, Naval Postgraduate School Thesis, 1993.

Medwin, H., E. Childs, E. A. Jordon, and R. A. Spaulding, Jr., "Sound scatter and shadowing at a seamount: Hybrid physical solutions in two and three dimensions," *Journal of the Acoustical Society of America*, 75 (1984), 1478-1490.

Naval Research Laboratory Report 8721, *NRL Reverberation Model: A Computer Program for the Prediction and Analysis of Medium- to Long-Range Boundary Reverberation*, by E. R. Franchi, J. M. Griffin, and B. J. King, Washington, D. C., 2 May 1984.

Norsk Polarinstitutt Nr. 37, *Shallow geology and geophysics of the Barents Sea*, by A. Elverhøi and A. Solheim, Oslo, Norway, 1987.

O'Keefe, S., "...From the Sea: preparing the naval service for the 21st century: a new direction for the naval service," U.S. Navy, 1992.

Planning Systems Incorporated Technical Report TR-S200, *Vertical Line Array Volume Reverberation Measurement System Study Findings*, by A. G. DiLoreto and M. Bradley, Slidell, Louisiana, April 1992.

Therrien, Charles W., *Discrete Random Signals and Statistical Signal Processing*, Prentice Hall, Englewood Cliffs, New Jersey, 1992.

Tolstoy, Ivan, and C. S. Clay, *Ocean Acoustics: Theory and Experiment in Underwater Sound*, American Institute of Physics, New York, 1987.

U.S. Navy Air Systems Command NAVAIR 28-SSQ-500-2, *Sonobuoy/SUS Pocket Card*, February 1989.

Urick, R. J., "Handy Curves for Finding the Source Level of an Explosive Charge Fired at a Depth in the Sea," *Journal of the Acoustical Society of America*, 49 (1971), 935-936.

Urick, Robert J., *Principles of Underwater Sound*, 3rd ed., McGraw-Hill Book Co., New York, 1983.

Weston, D. E., "Underwater Explosions as Acoustic Sources," *Proceedings of the Physical Society of London*, 76(Pt. 2) (1960), 233-249.

Woods Hole Oceanographic Institution Technical Report WHOI-92-44, *Array Data Acquisition with Wireless LAN Telemetry as applied to Shallow Water Tomography in the Barents Sea*, by K. von der Heydt, J. Kemp, J. Lynch, J. Miller, and C. -S. Chiu, Woods Hole, Massachusetts, December 1992.

Ziomek, Lawrence J., *Fundamentals of Acoustic Field Theory and Space-Time Signal Processing*, unpublished manuscript, 1993.

INITIAL DISTRIBUTION LIST

		No. Copies
1.	Defense Technical Information Center Cameron Station Alexandria, Virginia 22304-6145	2
2.	Library, Code 52 Naval Postgraduate School Monterey, California 93943-5101	2
3.	Department Chairman, Code EC Department of Electrical and Computer Engineering Naval Postgraduate School Monterey, CA 93943-5121	1
4.	Prof. J. H. Miller, Code EC/Mr Department of Electrical and Computer Engineering Naval Postgraduate School Monterey, CA 93943-5121	5
5.	Prof. C. S. Chiu, Code OC/Ci Department of Oceanography Naval Postgraduate School Monterey, CA 93943	1
6.	LT C. E. Muggleworth, USN 12 Peppermill Dr. Cherry Hill, NJ 08002	1
7.	Dr. J. F. Lynch Woods Hole Oceanographic Institution Woods Hole, MA 02543	1
8.	Dr. W. Jobst NAVOCEANO Code 0 Stennis Space Center, MS 39522	1

9.   Dr. T. Curtin   1
       Office of Naval Research
       800 North Quincy Street
       Arlington, VA 22217-5000

10.   Dr. M. Badiey   1
       Office of Naval Research
       800 North Quincy Street
       Arlington, VA 22217-5000

11.   Mr. John Schuster   1
       CNO Code N87T
       Submarine Security and Technology Branch
       Room 4D534
       Pentagon
       Washington, DC 20350

12.   CDR John Polcari   1
       PEO (USW) ASTO
       Undersea Warfare
       2531 Jefferson Davis Highway
       Arlington, VA 22242-5169